PERGAMON Mathematical and Computer Modelling 35 (2002) 517–547

MATHEMATICAL AND COMPUTER MODELLING

www.elsevier.com/locate/mcm

Micro- and Macro-Simulation of Freeway Traffic

D. HELBING*
Institute for Economics and Traffic, Dresden University of Technology
Andreas-Schubert-Str. 23, D-01062 Dresden, Germany
http://www.helbing.org/

A. HENNECKE AND V. SHVETSOV
II. Institute of Theoretical Physics, University of Stuttgart
Pfaffenwaldring 57/III, D-70550 Stuttgart, Germany

M. TREIBER
Institute for Economics and Traffic, Dresden University of Technology
Andreas-Schubert-Str. 23, D-01062 Dresden, Germany
http://www.mtreiber.de/

Abstract—We present simulations of congested traffic in circular and open systems with a nonlocal, gas-kinetic-based traffic model and a novel car-following model. The model parameters are all intuitive and can be easily calibrated. Micro- and macro-simulations with these models for identical vehicles on a single lane produce the same traffic states, which also qualitatively agree with empirical traffic observations. Moreover, the phase diagrams of traffic states in the presence of bottlenecks for the microscopic car-following model and the macroscopic gas-kinetic-based model almost agree. In both cases, we found metastable regimes, spatially coexistent states, and a small region of tristability. The distinction of different types of vehicles (cars and long vehicles) yields additional insight and allows us to reproduce empirical data even more realistically, including the observed fluctuation properties of traffic flows like the wide scattering of congested traffic data.

Finally, as an alternative to the gas-kinetic approach, we propose a new scheme for deriving nonlocal macroscopic traffic models from given microscopic car-following models. Assuming identical (macroscopic) initial and boundary conditions, we show that there are microscopic models for which the corresponding macroscopic version displays an almost identical dynamics. This enables us to combine micro- and macro-simulations of road sections by simple algorithms, and even to simulate them simultaneously.

Keywords—Congested traffic flow, Vehicle queues, Phase diagram, Micro-macro link, Car-following model.

1. INTRODUCTION

In recent years, the community of scientists engaged in traffic modelling has been rapidly growing (for overviews, see [1–3]). This is not only due to practical implications for optimizing freeway traffic [4], but also because of the observed nonequilibrium phase transitions [5,6] and the various nonlinear dynamical phenomena like the formation of traffic jams [7], stop-and-go traffic [8–10],

*This manuscript was written at the Collegium Budapest-Institute for Advanced Study, where D.H. had the pleasure to experience a fantastic hospitality and research atmosphere.

The authors want to express thanks for financial support by the BMBF (Research Project SANDY, Grant No. 13N7092) and by the DFG (Grant No. He 2789). They are also grateful to H. Taale and the Dutch Ministry of Transport, Public Works and Water Management for supplying the freeway data.

0895-7177/02/$ - see front matter Typeset by $\mathcal{A}\mathcal{M}\mathcal{S}$-TEX
PII: S0895-7177(01)00180-7

and "synchronized" congested traffic [5,11,12]. It seems that all forms of congested traffic have almost universal properties which are largely independent of the initial conditions and the spatially averaged density, like the characteristic outflow Q_{out} from traffic jams of about 1800 ± 300 vehicles per hour and lane or their typical dissolution velocity C of about -15 ± 5 kilometers per hour [13]. This universality arises from the highly correlated state of motion produced by traffic congestion. In particular, the outflow Q_{out} is related to the time gap between successive departures from the traffic jam [14,15]. Therefore, the outflow is practically independent of the initial conditions and the kind of congested traffic. As a consequence of the constant outflow, the propagation velocity C of jam fronts, given by the dissolution speed of traffic jams, is nearly constant as well.

From a physics point of view, a model for a real system (here, for unidirectional freeway traffic) should be as simple as possible, but not simpler (i.e., parameter dependencies that are known to exist should be reflected by the model). The parameters of the model should be intuitive, easy to calibrate, and the corresponding values should be realistic. Moreover, the traffic model should reproduce all observed localized and extended traffic states [16], including synchronized traffic and the wide scattering of congested traffic data [11]. Furthermore, the observed hysteresis effects [17,18], complex states [11,19], and the existence of self-organized quantities like the constant propagation velocity of stop-and-go waves or the outflow from a traffic jam [10] should be reproduced. Finally, the dynamics must not lead to vehicle collisions or exceed the maximum vehicle density, and the model should allow for a fast numerical simulation.

In this paper, we discuss some of these criteria for the recently proposed nonlocal, gas-kinetic-based traffic model (GKT model) [12,20] and the microscopic intelligent-driver model (IDM) [21]. In particular, we discuss several different kinds of bottlenecks and present the phase diagram of congested traffic states for open, inhomogeneous systems [22]. We show that, for identical vehicles, the macroscopic dynamics is qualitatively the same for both models. Finally, we investigate heterogeneous (mixed multiclass traffic composed of cars and lorries/long vehicles) and propose a natural explanation of the observed wide scattering of congested traffic data.

2. MACROSCOPIC TRAFFIC MODELS

In contrast to microscopic traffic models, which delineate the positions $x_\alpha(t)$ and velocities $v_\alpha(t)$ of all interacting vehicles α, macroscopic traffic models restrict to the description of the collective vehicle dynamics in terms of the spatial vehicle density $\rho(x,t)$ and the average velocity $V(x,t)$ as a function of the freeway location x and time t. One advantage of macroscopic traffic models is that they allow us to simulate the traffic dynamics in several lanes by effective one-lane models considering a certain probability of overtaking. In the following, we will use this approach, although it is also possible to develop macroscopic traffic models for several lanes with explicit treatment of lane-changing, as mentioned later on.

Being a consequence of the conservation of the number of vehicles, virtually all macroscopic traffic models are based on the continuity equation

$$\frac{\partial \rho}{\partial t} + \frac{\partial(\rho V)}{\partial x} = \nu(x,t), \tag{1}$$

for the vehicle density $\rho(x,t)$. The source term $\nu(x,t)\,dx$ is the rate of vehicles entering or leaving the freeway at on- or off-ramp sections of length dx. The differences between the various existing macroscopic traffic models mainly concern the equation for the average vehicle velocity $V(x,t)$. The Lighthill-Whitham model [23,24] and its variants [25–29] assume the equilibrium relation $V(x,t) = V_e(\rho(x,t))$. For the description of emergent traffic jams and stop-and-go traffic, however, one needs a dynamic velocity equation. Most proposals can (in their continuous form)

be summarized by the velocity equation

$$\frac{\partial V}{\partial t} + \underbrace{V\frac{\partial V}{\partial x}}_{\text{Transport term}} + \underbrace{\frac{1}{\rho}\frac{\partial P}{\partial x}}_{\text{Pressure term}} = \underbrace{\frac{1}{\tau}(V_e - V)}_{\text{Relaxation term}}. \tag{2}$$

Their main difference is the specification of the traffic pressure P, the relaxation time τ, and the dynamic equilibrium velocity V_e, which depends on the local vehicle density ρ. Notice that the Lighthill-Whitham model results in the limit $\tau \to 0$. Payne's [30] and Papageorgiou's [31] model is obtained for $P(\rho) = [V_0 - V_e(\rho)]/(2\tau)$, with the "free" or "desired" average velocity $V_0 = V_e(0)$. For $\frac{dP}{d\rho} = -\rho/[2\tau(\rho+\kappa)]\frac{dV_e}{d\rho}$, one ends up with Cremer's [32] model. In the model of Phillips [33], there is $P = \rho\theta$, where θ denotes the velocity variance. The model of Kühne [8,9], Kerner and Konhäuser [7], and Lee *et al.* [34] (KKKL model) results for $P = \rho\theta_0 - \eta\frac{\partial V}{\partial x}$, where θ_0 is a positive constant and η some viscosity coefficient. In comparison with a similar model by Whitham [35], the contribution $-\eta\frac{\partial V}{\partial x}$ implies an additional viscosity term $(\eta/\rho)\frac{\partial^2 V}{\partial x^2}$. This is essential for smoothing shock fronts, which is desirable from empirical and numerical points of view (but causes some inconsistencies for large density or velocity gradients [36], which can be avoided by a *nonlocal* macroscopic traffic model [37]).

Many of the above-mentioned models have proved their value in various applications, but they have been seriously criticized by Daganzo [36] because of theoretical inconsistencies. Apart from that, it is hard to decide which model is the best one. Whereas classical approaches focused on reproducing the empirically observed velocity-density relation and the regime of unstable traffic flow, recent publications pointed out that it is more important to have traffic models which are able to describe the observed spectrum of nonlinear phenomena and their characteristic properties [7,10,13,20,38,39]. We think that it would be desirable to develop models that reproduce both aspects of empirical data. In the following, we will propose such a macroscopic traffic model, which is theoretically consistent as well [40,41].

2.1. The Nonlocal, Gas-Kinetic-Based Traffic Model (GKT Model)

We derived macroscopic traffic equations from a gas-kinetic (Boltzmann-like) traffic model that was obtained from a simple microscopic car-following model under the approximation of quasi-instantaneous braking interactions [2,20] (which will be circumvented by the micro-macro link suggested in Section 4). Boltzmann-like traffic models for the spatiotemporal evolution of the so-called phase space density (= vehicle density $\rho(x,t)$ times velocity distribution $d(v;x,t)$) [4,33,40–50] go back to Prigogine and coworkers (for an overview, see [42]). Paveri-Fontana improved Prigogine's model and cured some of its inconsistencies [43]. Our gas-kinetic model can be viewed as an extension of Paveri-Fontana's equations to Enskog-like equations which are also valid in the regime of moderate and dense traffic, since they take into account the finite space requirements of vehicles. In particular, the equations become nonlocal to account for the fact that drivers react to the traffic situation ahead of them. This makes the derivation of the macroscopic traffic equations much more difficult than for the previous gas-kinetic models, the validity of which was limited to low vehicle densities. Therefore, our first calculations assumed "vehicular chaos" (i.e., uncorrelated vehicle velocities) and a gradient expansion in the vehicle density $\rho(x,t)$, average velocity $V(x,t) = \int dv\, v\, d(v;x,t)$, and velocity variance $\theta(x,t) = \int dv\, [v - V(x,t)]^2\, d(v;x,t)$ [41]. In this way, we could derive necessary high-density corrections of the traffic pressure $P(x,t) = \rho(x,t)\theta(x,t)$ (avoiding that vehicles would otherwise accelerate into jammed regions), and we could derive a plausible viscosity term, which had to be introduced in a phenomenological way in previous macroscopic traffic models. Meanwhile, we managed to carry out the calculations without a gradient expansion or other approximations [20,51,52], and even velocity correlations r among successive vehicles could be taken into account [53] (see Section 2.7). We have also generalized our model to a multiclass multilane model [2,53], which

allows us to account for different kinds of driver-vehicle units and lane changes in an explicit way. However, the results obtained up to now indicate that an efficient one-lane model (which averages over the neighboring lanes and the different driver-vehicle classes) can already capture the macroscopic vehicle dynamics in a semiquantitative way [2,53,54]. Nevertheless, in order to reproduce fluctuation effects like the wide scattering of congested flow-density data [1,11], it is necessary to take the diversity of driver-vehicle types into account [55] (see Sections 2.5 and 3.8).

In the following, we will discuss the efficient one-lane version of our nonlocal, gas-kinetic-based traffic model for the case of uncorrelated vehicle velocities, but we will come back to correlation effects later on. The results of our excessive calculations can be represented in terms of the continuity equation (1) and the velocity equation (2), but with a nonlocal, *dynamical* equilibrium velocity V_e that depends on the vehicle density and other macroscopic quantities at the actual vehicle location x and at the advanced "interaction point" x',

$$V_e = V_0 - \underbrace{\tau\left[1 - p\left(\rho'\right)\right]\chi\left(\rho'\right)\rho' B(\Delta V, S)}_{\text{Braking term}}. \tag{3}$$

Apart from other things, this implies that V_e implicitly depends on the (usually finite) variance θ and on the gradients of macroscopic variables like the density. A prime indicates that the corresponding variable is taken at the interaction point $x' = (x + s)$ rather than at the actual position x. For simplicity, we have assumed the safe distance s to increase linearly with the average vehicle velocity V,

$$s = \gamma\left(\frac{1}{\rho_{\max}} + TV\right), \tag{4}$$

where $\rho_{\max}$ denotes the maximum vehicle density, $T \approx 1.8\,\mathrm{s}$ the safe time headway, and $\gamma \approx 1$ an anticipation factor.

The "Boltzmann factor"

$$B(\Delta V, S) = S\left\{\Delta V N(\Delta V) + \left[1 + (\Delta V)^2\right] E(\Delta V)\right\}, \tag{5}$$

in which

$$N(y) = \frac{\mathrm{e}^{-y^2/2}}{\sqrt{2\pi}} \tag{6}$$

represents the normal distribution and

$$E(y) = \int_{-\infty}^{y} dz\, \frac{\mathrm{e}^{-z^2/2}}{\sqrt{2\pi}}, \tag{7}$$

the Gaussian error function, describes the dependence of the braking interaction on the effective dimensionless difference ΔV between the velocities at the actual position and the interaction point. The effective velocity difference is defined by

$$\Delta V = \frac{V - V'}{\sqrt{S}}, \tag{8}$$

where

$$S = \theta + \theta'. \tag{9}$$

Hence, apart from the velocity difference to the interaction point, ΔV also takes into account the velocity variances θ and θ' at the actual vehicle position x and the interaction point x', respectively. In spatially homogeneous traffic, we have $B(0, S) = S/2$. In the limiting case $\Delta V \gg 0$, where the preceding cars are much slower, we have a much stronger interaction $B(\Delta V, S) = (\Delta V)^2 S$. If, in contrast, the preceding cars are much faster (i.e., $\Delta V \ll 0$), we have $B(\Delta V, S) \approx 0$.

That is, since the distance is increasing, then the vehicle at position x will not brake, even if its headway is smaller than the safe distance.

Notice that, for $\gamma = 1$, the macroscopic interaction term can be easily understood by the underlying microscopic dynamics of the gas-kinetic-based traffic model. If a vehicle at location x with velocity v is faster than one at x' with velocity w (i.e., $\Delta v = v - w > 0$), it approaches the car in front within the time $\Delta t = \Delta x_{\text{free}}/\Delta v$, where $\Delta x_{\text{free}} = 1/(\rho'\chi')$ is the average interaction-free distance per car. Then, if it cannot overtake immediately, which would happen with probability $(1 - p')$, it abruptly reduces the velocity by Δv. The resulting ensemble-averaged deceleration is

$$\left\langle \frac{\Delta v}{\Delta t} \right\rangle = -(1-p')\,\chi'\rho' \int_0^\infty d(\Delta v)\,(\Delta v)^2\, d_\Delta(\Delta v). \tag{10}$$

If v and w are Gaussian distributed with averages V, V', and variances θ, θ', respectively, the distribution function $d_\Delta(\Delta v)$ of the velocity difference Δv is Gaussian distributed, with expectation value $(V - V') = \sqrt{S}\,\Delta V$ and variance S. Evaluating integral (10) yields $\langle \Delta v/\Delta t \rangle = -(1-p')\chi'\rho' B(\Delta V, S)$, i.e., the macroscopic braking term in equation (3).

Next, we will specify the pressure relation. Similar to gases, the calculations give

$$P = \rho[\theta + W(\rho)] \tag{11}$$

(see [2,56]). Again,

$$\theta = \langle \theta_i \rangle = \sum_{i=1}^{I} \frac{\rho_i}{I\rho}\,\theta_i \tag{12}$$

is the (weighted) average of the lane-specific velocity variances θ_i, where the weights are the relative densities $\rho_i/(I\rho)$ in the I different lanes i. The monotonically decreasing, density-dependent function

$$W = \langle (V_i - V)^2 \rangle = \sum_{i=1}^{I} \frac{\rho_i}{I\rho}(V_i)^2 - \left(\sum_{i=1}^{I} \frac{\rho_i}{I\rho} V_i \right)^2 \tag{13}$$

can be used to correct for the variation of the average velocities V_i in the different lanes (see Figure 1a), but it is often neglected.

The pressure term describes the kinematic dispersion of the macroscopic velocity in inhomogeneous traffic as a consequence of the finite velocity variance. For example, the macroscopic velocity in front of a small vehicle cluster will increase *even if no individual vehicle accelerates*, because the faster cars will leave the cluster behind. The kinematic dispersion also leads to a smooth density profile at the dissolution front between congested traffic and an empty road, as it occurs when a road blockage is removed (see Figure 2 and [37]).

Notice that the total variance

$$\Theta = (\theta + W) \tag{14}$$

decreases with density and vanishes at the maximum vehicle density $\rho_{\max}$. Therefore, the density-gradient $\frac{dP}{d\rho}$ of the traffic pressure P may decrease with growing density and increase with decreasing density. Hence, according to the pressure term $(1/\rho)\,\frac{\partial P}{\partial x}$, it seems that vehicles would accelerate into denser regions and decelerate when driving into regions of lighter traffic. This tendency, however, is overcompensated for by the nonlocal interaction term [41]. Because of its nonlocality, the braking term in relation (3) strongly increases with the density gradient. This can be more explicitly seen by applying the gradient expansions $\rho' \approx \rho + s\,\frac{\partial \rho}{\partial x} + \cdots$, etc.

Next, in order to close the system of equations, one needs to specify the dynamics of the velocity variance θ. It turned out that, for a description of the presently known properties of traffic flows, we do not need to describe the variance by the associated partial differential equation. It seems sufficient to describe the variance by the equilibrium relation

$$\theta = D\tau \tag{15}$$

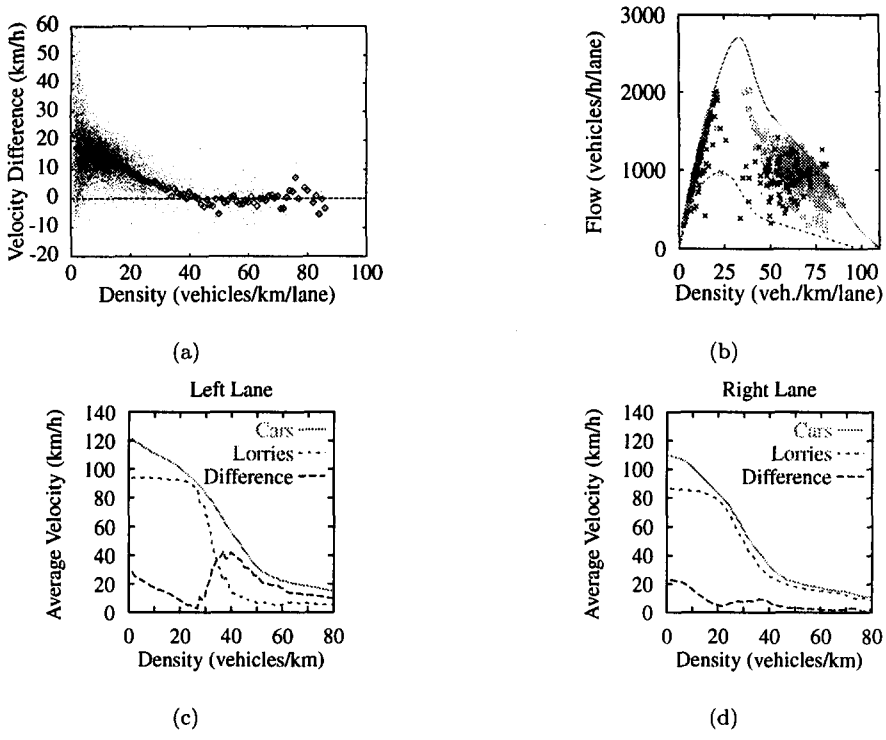

Figure 1. (a) Difference between the average velocity $V_2(\rho)$ in the left lane and $V_1(\rho)$ in the right lane as a function of the lane-averaged vehicle density ρ. Points correspond to one-minute data from November 2, 1994, which were determined from single-vehicle data of the Dutch freeway A9. We find no gap in the data cloud, so that there is no support for the hypothesis of a phase transition to synchronization among lanes. The same conclusion can be drawn from the averages of the one-minute data belonging to the same density, which are represented by diamonds. We find a linear decrease without discontinuities up to a density of 40 vehicles per kilometer and lane, above which the velocity in both lanes is the same. (b) The displayed points in flow-density space correspond to lane-averaged one-minute data (dark crosses) and related simulation results (grey boxes) at the location of an on-ramp (after [55]). The simulations manage to reproduce both the quasi-linear flow-density relation at small densities and the scattering of the data over a two-dimensional region in so-called "synchronized" congested traffic at medium and high densities. The simulations are based on the assumption that, in an effective model of mixed traffic, the time-dependent parameters $X(t)$ are given by a linear interpolation $X(t) = \{p_{\rm lo}(t)X_{\rm lo} + [1 - p_{\rm lo}(t)]X_{\rm car}\}$ between the parameters $X_{\rm car}$ of cars and $X_{\rm lo}$ of lorries, where $p_{\rm lo}(t)$ denotes the time-dependent fraction of long vehicles passing the cross section. By lines, we have displayed the assumed equilibrium flow-density relations for traffic consisting of 100% cars (—), and of 100% long vehicles (- - -). (c),(d) Average velocities of cars and lorries (long vehicles) in the left and the right lane as a function of density. The difference of these empirical curves shows a minimum around 25 vehicles per kilometer, where cars are almost as slow as lorries (after [6]). However, at higher densities, cars are faster again, which shows that there must be overtaking maneuvers at medium and high densities, which does not support the hypothesis of synchronization among lanes.

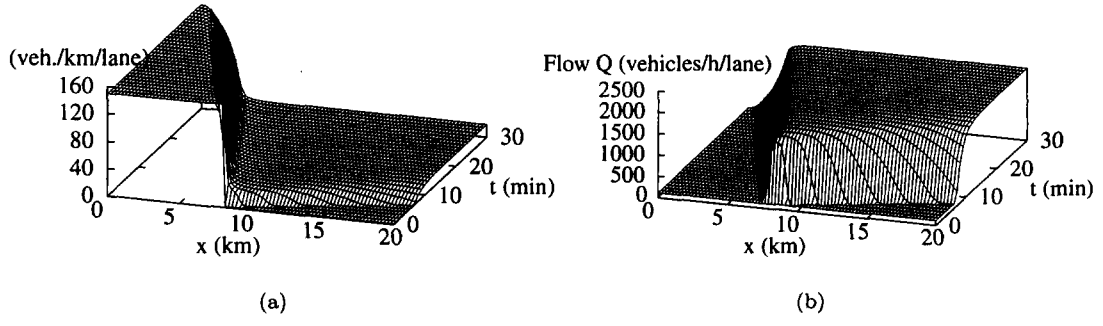

Figure 2. Simulation of a downstream front with a jam density of 140 vehicles/km/lane. Shown is the spatiotemporal development (a) of the density $\rho(x,t)$, and (b) the flow $Q(x,t) = \rho(x,t)V(x,t)$. Free boundary conditions were used on both sides.

of the dynamical variance equation [54], where D denotes a velocity diffusion coefficient which is a function of the vehicle density ρ and the average velocity V. Empirical data suggest that the variance is a density-dependent fraction $A(\rho)$ of the squared average velocity [20,41],

$$\theta = A(\rho)V^2. \tag{16}$$

This guarantees that the velocity variance will vanish if the average velocity goes to zero, as required, but it will be finite otherwise. It turns out that the variance prefactor A is higher in congested traffic than in free traffic (Figure 3a). The empirical data can be approximated by the Fermi function

$$A(\rho) = A_0 + \Delta A \left[\tanh\left(\frac{\rho - \rho_c}{\Delta\rho}\right) + 1\right], \tag{17}$$

where A_0 and $A_0 + 2\Delta A$ are about the variance prefactors for free and congested traffic, respectively, ρ_c is roughly of the order of the critical density for the transition from free to congested traffic, and $\Delta\rho$ denotes the width of the transition region.

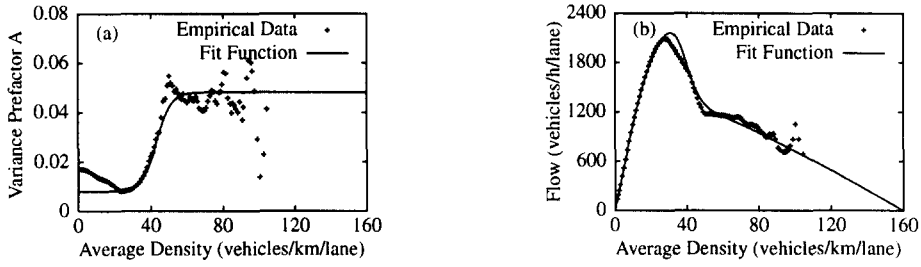

(a) (b)

Figure 3. Comparison of (a) the density-dependent relative variance Θ in units of the squared average velocity, and (b) the equilibrium flow-density relation (21) of our gas-kinetic-based traffic model (solid lines) with empirical data (crosses). The empirical data were obtained from single-vehicle data of the Dutch motorway A9 (where a speed limit of 120 km/h applies), by averaging over one-minute intervals. Note that both the variance-density relation and the velocity-density relation in equilibrium are fitted by a single, density-dependent function $A(\rho)$. It turns out that the deviation of the variance-density relation from the empirical data at small densities is not of great importance for the dynamics of the traffic model. It can, however, be accounted for by the function $W(\rho)$; see formulas (13) and (14).

Finally, we will specify the "effective cross section" $(1-p)\chi = (1-p)/p$, assuming that the average time headway of vehicles corresponds to the safe time headway T, if the vehicle density is high (i.e., the freeway space is almost used up completely by the vehicular space requirements). This specification means that, in dense and homogeneous traffic situations with $V' = V$ and $\theta' = \theta$, we should have $s = 1/\rho = [1/\rho_{\max} + TV_e(\rho)]$, where we insert the equilibrium solution (19). This gives us the relation

$$[1 - p(\rho)]\chi(\rho) = \frac{V_0 \rho T^2}{\tau A(\rho_{\max})(1 - \rho/\rho_{\max})^2}, \tag{18}$$

which also makes sense in the low-density limit $\rho \to 0$, since it implies $\chi \to 1$ and $p \to 1$.

2.2. Properties of the Nonlocal, Gas-Kinetic-Based Traffic Model

Summarizing the above results, our gas-kinetic-based traffic model can be written in the general form (1),(2) of macroscopic traffic models, but with a nonlocal relaxation term. Since the equations are structurally related to, for example, the KKKL model, we find many similar nonlinear phenomena [20]. This includes the sequence of stable, linearly unstable, and metastable regimes [10,57], the local breakdown effect [58], the local cluster effect [10], and, at sufficiently large densities, the formation of so-called dipole layers [57]. The response of equilibrium traffic to

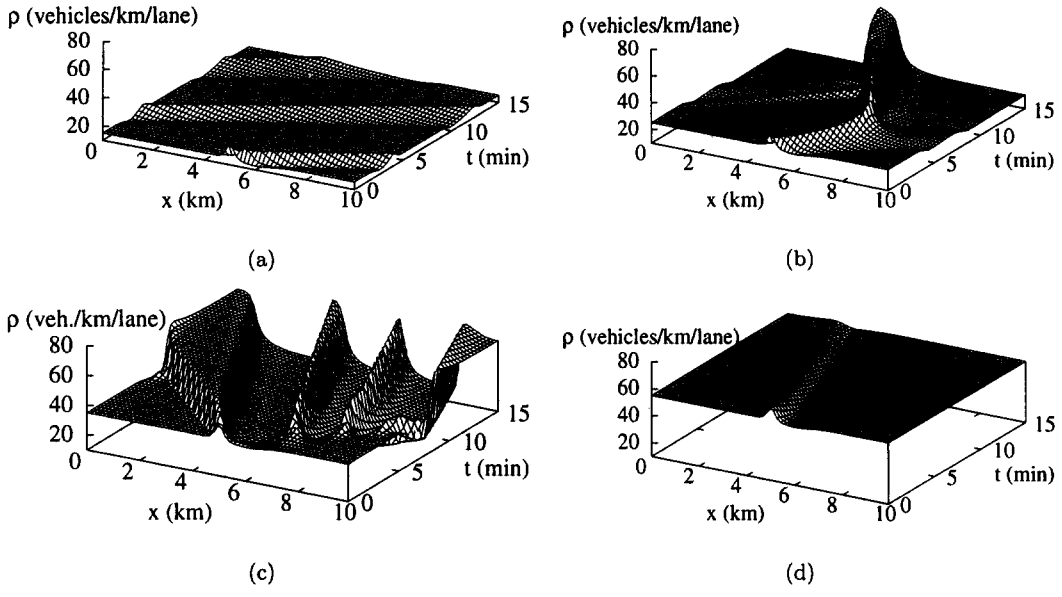

Figure 4. Spatiotemporal evolution of the traffic density $\rho(x,t)$ on a unidirectional ring of circumference 10 km, starting with homogeneous traffic to which a localized initial perturbation of amplitude 10 vehicles/km/lane is added. (a) Free and stable traffic at an average density of 15 vehicles/km/lane, (b) metastable traffic for 25 vehicles/km/lane, (c) unstable traffic for 35 vehicles/km/lane, (d) stable congested traffic for 55 vehicles/km/lane. The chosen model parameters are displayed in Table 1.

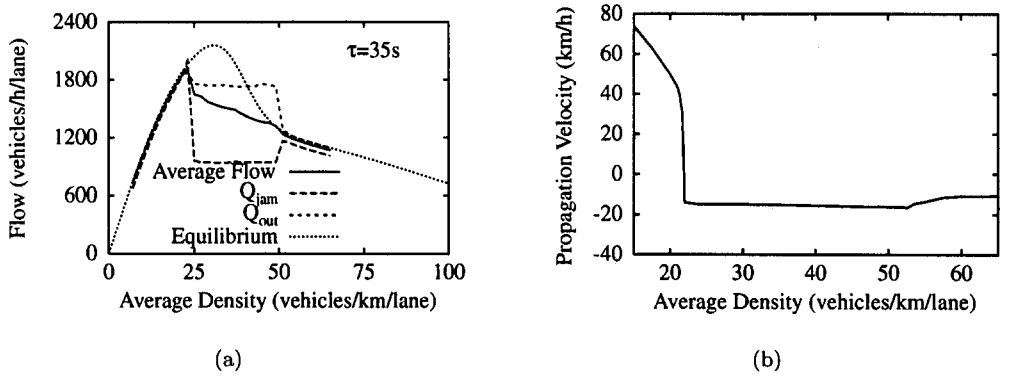

Figure 5. (a) Characteristic flows resulting in fully developed stop-and-go traffic on a circular road, as a function of the spatially averaged density. Depicted are the flows Q_{jam} in the jammed regions (– –), the outflows Q_{out} from jams (- - -), and the average flows (—). For comparison, the equilibrium flow $Q_{\mathrm{e}}(\rho) = \rho V_{\mathrm{e}}(\rho)$ with $V_{\mathrm{e}}(\rho)$ from equation (19) is also shown (· · ·). Notice that, in the unstable range, the average *dynamic* flow is lower than the equilibrium flow. (b) Propagation velocity of density clusters as a function of average density. We started our simulations with an initial perturbation of amplitude 10 vehicles/km/lane and measured the group velocity after a sufficiently long transient time. The propagation velocity at low densities is positive, but slower than the average vehicle velocity. In the instability region, the negative propagation velocity of fully developed traffic jams (i.e., their dissolution velocity) is independent of the initial density, and its magnitude is in agreement with empirical data. Notice that the dissolution velocity C of jam fronts corresponds to the slope of the average flow depicted in (a).

localized disturbances is similar to the Kerner-Konhäuser model [58]. More specifically, for densities below a certain critical density ρ_{c1} and above some density ρ_{c4}, homogeneous traffic is stable with respect to localized perturbations (Figures 4a and 4d), and for a range $\rho_{\mathrm{c2}} < \rho < \rho_{\mathrm{c3}}$ of intermediate densities, it is linearly unstable, giving rise to cascades of traffic jams ("stop-and-go traffic", cf., Figure 4c). For the two density regimes $\rho_{\mathrm{c1}} \leq \rho \leq \rho_{\mathrm{c2}}$ and $\rho_{\mathrm{c3}} \leq \rho \leq \rho_{\mathrm{c4}}$ between the stable and the linearly unstable regions, traffic is metastable; i.e., it behaves unstable with respect to perturbations exceeding a certain critical amplitude $\Delta\rho_{\mathrm{cr}}(\rho)$ (Figure 4b), but otherwise stable. For the self-organized density ρ_{jam} inside traffic jams, we find a typical value $\rho_{\mathrm{jam}} \geq \rho_{\mathrm{c4}}$ [20].

Furthermore, there exists a range $\rho_{cv} < \rho < \rho_{c3}$ with $\rho_{cv} > \rho_{c2}$, where traffic is linearly unstable, but convectively stable; i.e., all perturbations grow, but they are eventually convected away in upstream direction [59].

In addition, we obtain that, in the unstable traffic regime, the resulting flow-density relation differs from the equilibrium one (lying below the latter). We also find that the outflow Q_{out} from traffic jams is independent of the initial conditions and the spatially averaged density (Figure 5a). Furthermore, the dissolution velocity C of traffic jams varies only a little with density (Figure 5b).

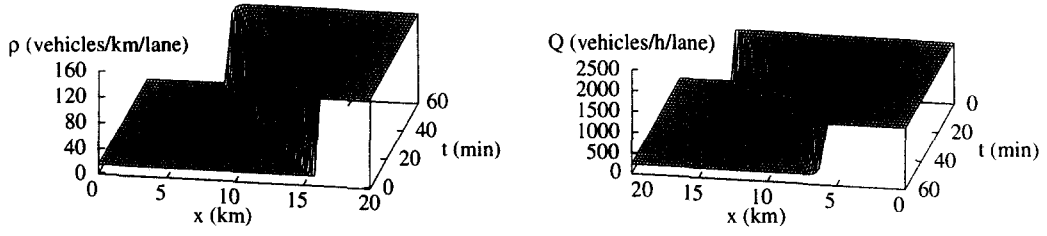

(a) (b)

Figure 6. Simulation of an upstream front with initial densities of $\rho_1 = 15$ vehicles/km/lane and $\rho_2 = 140$ vehicles/km/lane. Shown is the evolution of (a) the density $\rho(x,t)$, and (b) the flow $Q(x,t) = \rho(x,t)V(x,t)$. Note that, in contrast to other macroscopic traffic models [36], the simulations do *not* produce densities above ρ_{max} or negative flows. In (b), the direction of the space and time axes is reversed for illustrative reasons.

The main difference with respect to other macroscopic traffic models is the nonlocal character of the braking term. Nevertheless, our model can still be rewritten in the form of flux equations, with a nonlocal source term [51,52]. For this reason, we can apply various standard methods of numerical integration. It turns out that the nonlocal term has similar smoothing properties like a viscosity term. However, its effect is anisotropic due to the anticipation behavior in forward direction reflecting that vehicles mainly react on density or velocity gradients ahead of them, not behind them (compare Figure 6 with Figure 2). Compared to a viscosity term, the nonlocality does not change the hyperbolic character of the partial differential equations to a parabolic one. Therefore, it has favourable properties with respect to numerical stability and integration speed [37]. As a consequence, our model allows a robust real-time simulation of freeway stretches up to several thousand kilometers on a usual PC.

2.3. Model Calibration and Validation

It turns out that our model can be easily calibrated to the static and dynamic properties of traffic flow data by a systematic procedure. In spatially homogeneous traffic, the average velocity relaxes to

$$V_e(\rho) = \frac{\tilde{V}^2}{2V_0}\left(-1 + \sqrt{1 + \frac{4V_0^2}{\tilde{V}^2}}\right), \tag{19}$$

with

$$\tilde{V}(\rho) = \sqrt{\frac{V_0}{\tau[1-p(\rho)]\chi(\rho)\rho A(\rho)}} = \frac{1}{T}\left(\frac{1}{\rho} - \frac{1}{\rho_{max}}\right)\sqrt{\frac{A(\rho_{max})}{A(\rho)}}. \tag{20}$$

This also determines the equilibrium traffic flow per lane by

$$Q_e(\rho) = \rho V_e(\rho), \tag{21}$$

which is depicted in Figure 3b. In the limit of small densities, we find $V_e(\rho) \approx V_0$, while in the limit of high densities (i.e., for $(1 - \rho/\rho_{max}) \ll 1$ or $V_e \ll V_0$), we have $V_e(\rho) \approx \tilde{V}(\rho)$; i.e., $V_e(\rho) \approx (1/\rho - 1/\rho_{max})/T$. Apparently, the equilibrium flow-density relation is only affected by

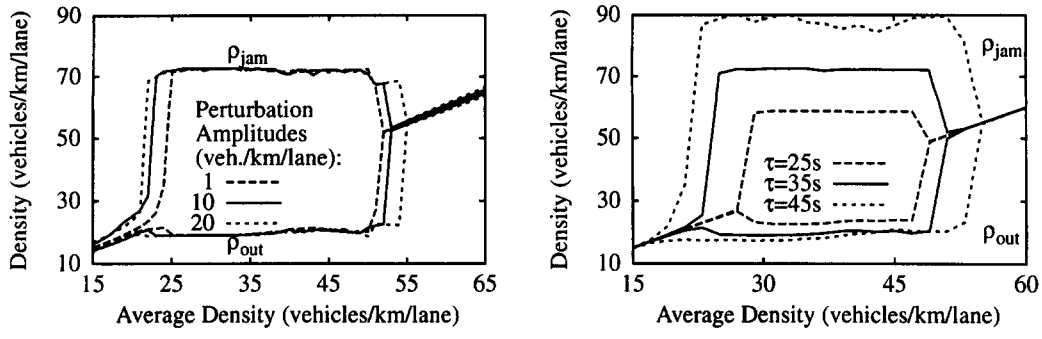

Figure 7. Stability diagram for a localized perturbation of homogeneous traffic on a ring of circumference 10 km. Both diagrams show the developing maximum and minimum densities ρ_{jam} and ρ_{out} as a function of the spatially averaged density, measured after a dynamical equilibrium was reached. The unstable traffic regime corresponds to the density range where the jam amplitude ($\rho_{\text{jam}} - \rho_{\text{out}}$) is large (rectangle-like shaped regions). Diagram (a) shows the dependence of the stability diagram on the perturbation amplitude $\Delta\rho$. One can clearly see two density ranges $[\rho_{c1}, \rho_{c2}]$ with $\rho_{c1} = 21$ vehicles/km/lane and $\rho_{c2} = 24$ vehicles/km/lane, and $[\rho_{c3}, \rho_{c4}]$ with $\rho_{c3} = 51$ vehicles/km/lane and $\rho_{c4} = 55$ vehicles/km/lane, where traffic is nonlinearly stable, i.e., stable for small perturbations, but unstable for large perturbations. In the range $[\rho_{c2}, \rho_{c3}]$, homogeneous traffic is unstable for arbitrary perturbation amplitudes. Diagram (b) shows the stability diagram for various relaxation times τ and a perturbation amplitude of $\Delta\rho = 1$ vehicle/km/lane.

the model parameters V_0, T, and $\rho_{\max}$. The desired velocity V_0 can be determined by fitting flow-density data at low densities by a straight line ρV_0, while the safe time headway T and the maximum density $\rho_{\max}$ are obtained by fitting the data at high densities by a straight line $(1 - \rho/\rho_{\max})/T$, which crosses the abscissa at $\rho_{\max}$ with a slope of $-1/(\rho_{\max} T)$.

The model parameters τ and γ influence the stability behavior. Figure 7 shows that an increased value of τ leads both to an increased range of *instability*, and to increased amplitudes ($\rho_{\text{jam}} - \rho_{\text{out}}$) of traffic jams. Further simulations showed that higher values of γ tend to increase the *stability* of traffic. This is plausible, since γ reflects the anticipation of future velocity changes. γ and τ also determine the shape and width of the downstream and upstream fronts connecting free and congested states (see Figures 2 and 6). Since τ and γ weakly influence the outflow Q_{out} from traffic jams, the calibration of T, τ, and γ is repeated recursively until an optimal fit of the model to the empirical data is achieved.

Because of their intuitive meaning, the plausible range of values for the model parameters is rather restricted. V_0 is given by the average free speed. $\rho_{\max}$ must be consistent with the average length of vehicles plus a reasonable bumper-to-bumper distance of about 1.5 m in standing traffic. T should be compatible with the average time headway kept in homogeneous congested traffic. Reasonable (average) time headways are in the range $T \in [1.0\,\text{s}, 2.5\,\text{s}]$. Initial accelerations $a_{\max} = V_0/\tau$ are typically in the range $a_{\max} \in [1\,\text{m/s}^2, 4\,\text{m/s}^2]$, corresponding to $\tau \in [10\,\text{s}, 40\,\text{s}]$. (Notice that, for $V_0 = 158\,\text{km/h}$, τ would have the meaning of the average acceleration time from 0 to 100 km/h.) Therefore, a relaxation time $\tau \approx 35\,\text{s}$ is reasonable for freeway traffic, whereas τ is smaller for city traffic. Finally, the minimum anticipation of traffic is to the car in front, implying $\gamma \geq 1$.

The above procedure of parameter calibration has been applied to single-vehicle data of the Dutch freeway A9, leading to the parameter set shown in Table 1. It turns out that all optimized parameters have realistic values. In particular, this holds for τ. The typical values for the safe time headway of $T = 1.8\,\text{s}$ is consistent with the rule "distance (in m) should not be less than half the velocity (in km/h)" suggested by German road authorities. For other data, however, one often finds that a somewhat smaller time headway yields a better fit.

Since the model parameters are meaningful, it is simple to model changes of the traffic dynamics caused by external effects like environmental influences (cf., Figure 8). For example, a speed limit

Table 1. Typical values of model parameters used in the nonlocal, gas-kinetic-based traffic model to reproduce empirical data of the Dutch freeway A9.

V_0	T	τ	$\rho_{\max}$	γ
110 km/h	1.8 s	35 s	160 veh./km	1.2

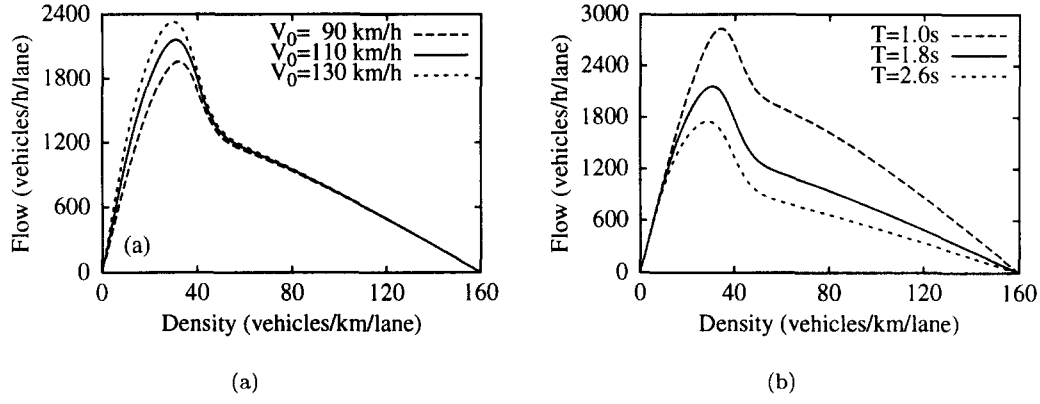

(a) (b)

Figure 8. Equilibrium flow-density relations of the nonlocal, gas-kinetic-based traffic model. The diagrams (a) and (b) show the variation with the model parameters V_0 and T, respectively. Notice that a reasonable speed limit almost does not affect the flow in the congested regime, while a variation of the following time t can account for large variations in the flow in the congested density regime. In each diagram, the solid lines correspond to the standard parameter set displayed in Table 1.

would be considered by decreasing V_0. Bad weather conditions leading to more defensive driving would be characterized by an increased time headway T and a lower value of V_0 (plus a reduction of γ, if there is heavy fog). In rush-hour traffic, it is plausible to assume a higher percentage of experienced drivers than in holiday traffic, which would correspond to a higher γ. Effects like a varying distribution of vehicle types can be modelled as well. For example, a higher proportion of lorries (long vehicles) would lead to a decrease of V_0 and $\rho_{\max}$, but also to an increased value of τ.

2.4. Treatment of Boundaries in Open Systems

Notice that the left-hand sides of the continuity equation (1) and the velocity equation (2) constitute a hyperbolic set of partial differential equations. Hence, the direction of information flow due to convective and dispersive processes is given by the characteristic lines [60]. Specifically, the velocities of information flow are given by

$$\lambda_{1,2} = V - \frac{1}{2\rho}\frac{\partial P}{\partial V} \pm \sqrt{\frac{1}{4\rho^2}\left(\frac{\partial P}{\partial V}\right)^2 + \frac{\partial P}{\partial \rho}}, \qquad \text{with } P(\rho, V) = \rho\theta(\rho, V). \tag{22}$$

For all physically reasonable parameter sets, they are always positive. Information flow *against* the direction of motion of the simulated vehicles is taken into account by the nonlocal interaction term. The consequences are as follows.

(i) There is always a transport of information in both directions, upstream and downstream.
(ii) The most suitable differencing scheme for the numerical integration is the upwind scheme (see [61]).

By choosing the upwind scheme, the downstream boundary conditions are only relevant for the nonlocal interaction term. This is in accordance with the boundary conditions for microscopic traffic simulations, where the first car at the downstream boundary always needs a "phantom" leading car for its update process. In particular, the microscopic downstream boundary conditions determine only the *acceleration* of this first car, but do not determine the *flow* of exiting vehicles.

At the same time, there always has to be a defined inflow of new vehicles at the upstream boundary. The same is true for the simulation of nonlocal macroscopic models with the upwind scheme. Therefore, it is no problem to formulate downstream boundary conditions which are always satisfied.

At the upstream boundary, unphysical situations can emerge when a backwards moving jam approaches the boundary, but the assumed boundary (in)flow is higher than the flow inside the traffic jam. Then, the equations are no longer well posed in a mathematical sense. Such situations may occur whenever there is a slight offset in the arrival times of simulated and real jams at the boundary. This means the boundary conditions have to be implemented in a way that, on one hand, copes with unexpected or offset density waves and, on the other hand, returns to the exact solution as soon as possible. This can be done by an algorithm that implements homogeneous von Neumann boundary conditions instead of Dirichlet boundary conditions for density and flow, if

(i) there is congested traffic in the vicinity of the boundary, and
(ii) the imposed inflow is larger than the traffic flow of the congested state [37].

Condition (i) means that, near the boundary, the local group velocity $v_g = \frac{\partial(\rho V_e(\rho))}{\partial\rho}$ for instantaneous velocity relaxation is negative, or

$$\rho(\delta, t) > \rho_m \tag{23}$$

(with some small $\delta > 0$ and ρ_m being the density for maximum equilibrium flow). Condition (ii) can be expressed by requiring

$$Q(0, t) > Q(\delta, t). \tag{24}$$

This algorithm has been tested as follows. First, we simulated a circular road of 20 kilometers in length. The simulated scenario contains a local dipole-like perturbation in the initial conditions which develops to a backwards moving cluster (see Figure 9a). Then we used the time-dependent results at the locations $x = 5\,\text{km}$ and $x = 15\,\text{km}$ as Dirichlet boundary conditions for the simulation of a new, ten kilometer long *open* system. Figure 9b shows a comparison of the density profiles of the two systems at two times t_1 and t_2. At $t_1 = 8\,\text{min}$, the cluster is not yet fully developed, and at $t_2 = 80\,\text{min}$, it has propagated around the circle once. The profiles belonging to the same time points agree so well, that they would lay one upon each other. For this reason, we have depicted them with a slight artificial offset. After this hard and successful test, we are prepared to simulate the traffic phenomena observed on real freeways, which are open systems.

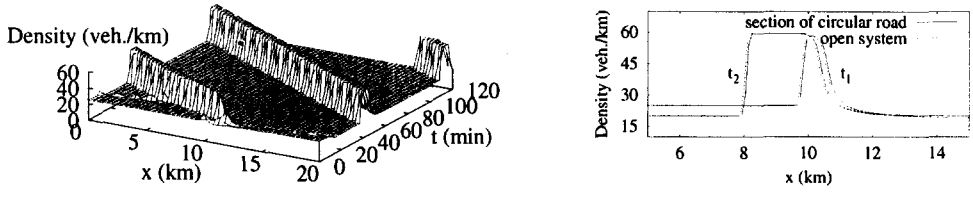

(a) (b)

Figure 9. (a) Circular reference system simulated in order to obtain boundary conditions for the simulation of a comparable open system. (b) Comparison of density profiles at two times $t_1 = 8\,\text{min}$ and $t_2 = 80\,\text{min}$, obtained in the circular reference system (solid) and in an open system which was simulated with boundary conditions taken from the reference scenario (dashed). In order to make the curves distinguishable, one of the profiles was shifted by 100 m.

2.5. Simulation of "Synchronized" Congested Traffic

Recently, Kerner and Rehborn [5] have presented experimental data indicating a first-order transition to "synchronized" congested traffic. Traffic data from several freeways in Germany [5,11], the Netherlands [2,54,55], and the United States [18,62] indicate that synchronized

traffic is the most common form of congested traffic. Synchronized traffic typically occurs at on-ramps when vehicles are added to already busy "freeways" and has the following properties.

(i) The dynamics of the average velocities on all lanes is highly correlated ("synchronized").
(ii) The corresponding points in the flow-density plane are widely scattered.
(iii) Synchronized traffic is characterized by a low average velocity, but, in contrast to traffic jams, the associated traffic flow is rather high.
(iv) The transition to synchronized traffic is often caused by a localized and short perturbation of traffic flow that starts downstream of the on-ramp and propagates upstream with a velocity of about $-10\,\mathrm{km/h}$.
(v) As soon as the perturbation passes the on-ramp, it triggers synchronized traffic which spreads upstream in the course of time.
(vi) Downstream, synchronized traffic eventually relaxes to free traffic.
(vii) Synchronized traffic often persists over several hours.
(viii) The transition from synchronized traffic to free traffic occurs at a lower density and higher average velocity than the inverse transition (*hysteresis effect*).

We believe that Property (i), i.e., the synchronization, requires a strong coupling among lanes. When the street becomes crowded, the drivers are trying to avoid obstructions by changing lanes. They fill developing gaps in the other lane until it becomes as slow as their own lane (Figure 1a), thereby balancing each upcoming disequilibrium among lanes. While restoring the balance is related to a considerable number of lane changes [53], the lane changing rate becomes rather low as soon as the synchronization among lanes is reached. This idea can be indirectly supported by empirical traffic data which show that, even in congested traffic, there can be a significant difference in the velocities of cars and lorries (Figures 1c and 1d), which can be only attributed to lane changing and overtaking.

Property (ii) seems to be the result of the diversity of vehicles [55], as demonstrated in Figure 1b. The other characteristic properties of "synchronized" traffic can be reproduced by the effective one-lane version of the nonlocal, gas-kinetic-based traffic model described above. This applies to homogeneous forms of "synchronized" traffic as well as to nonstationary forms (see oscillating congested traffic, OCT, discussed below). The essential point is that, along on-ramps (or off-ramps), there is a source term in the continuity equation (1). With

$$\nu = \frac{Q_{\mathrm{rmp}}}{nL}, \tag{25}$$

we assume that this source term is given by the actually observed inflow $Q_{\mathrm{rmp}} > 0$ from (or outflow $Q_{\mathrm{rmp}} < 0$ to) the ramp, divided by the merging length L and by the number n of lanes. The inflow has an upper limit that depends on the downstream flow on the main road [63]. If one likes to model the tendency that some on-ramp vehicles enter as soon as possible regardless of the length of the ramp, one replaces L by an effective ramp length $L^* < L$. Moreover, if the average velocity V_{rmp} of entering or leaving vehicles on the ramp is different from the average velocity V on the main road, this gives an additional contribution

$$\frac{\nu}{\rho}\,(V_{\mathrm{rmp}} - V) \tag{26}$$

to the right-hand side of the velocity equation (2), corresponding to a source term νV_{rmp} in the related differential equation for the traffic flow $Q = \rho V$ on the freeway [2,64]. However, usually one assumes $V_{\mathrm{rmp}} \approx V$.

Our simulations reproduced the observations (iii) to (viii) very realistically. For $V_{\mathrm{rmp}} = V$, the parameter values $V_0 = 128\,\mathrm{km/h}$, $\rho_{\max} = 160\,\mathrm{vehicles/km}$, $T = 1.6\,\mathrm{s}$, $\tau = 31\,\mathrm{s}$, $\gamma = 1.0$, and the observed boundary flows (Figure 10c), the simulated velocities and flows are, apart from

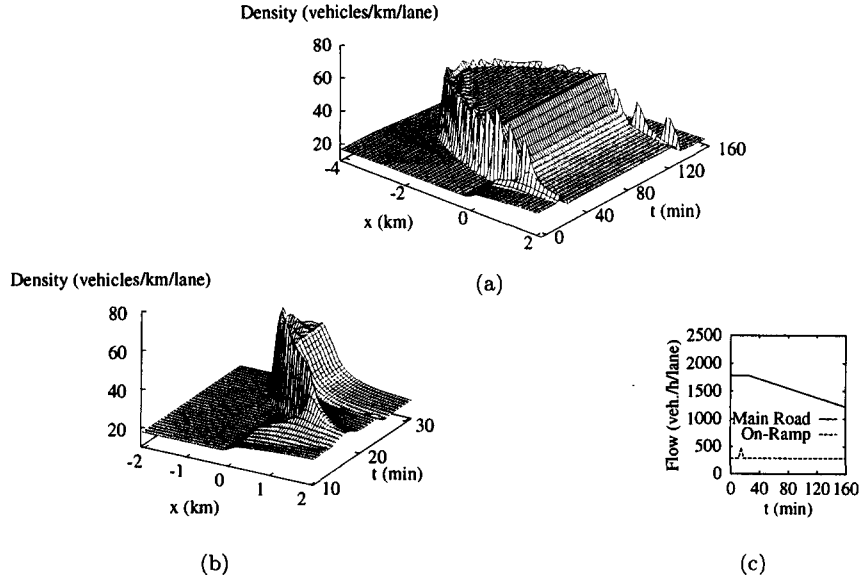

Figure 10. Spatiotemporal evolution of the lane-averaged density after a small peak of inflow from the on-ramp (after [12]). The on-ramp merges with the main road at $x = 0\,\mathrm{km}$ with a merging length of $L = 300\,\mathrm{m}$. Traffic flows from left to right. In (a), the parabolically shaped region of high density corresponds to "synchronized" congested traffic. Plot (b) shows the formation of this state in more detail. The time-dependent inflows Q_{main} at the upstream boundary and Q_{rmp}/n at the on-ramp are displayed in (c).

fluctuations, in good agreement with the empirical curves presented by Kerner and Rehborn (compare [12] with [5]).

Our results suggest the following interpretation of the phase transition to "synchronized" congested traffic. Initially, the homogeneous flow Q_{main} upstream of an on-ramp is stable, while the higher downstream flow $Q_{\mathrm{down}} = Q_{\mathrm{main}} + Q_{\mathrm{rmp}}/n$ is metastable. Without any disturbance of the main or ramp flow, free traffic flow will continue. However, a (positive or even a negative) perturbation in the on-ramp or the main flow will eventually cause a breakdown of velocity close to the on-ramp. Speaking in the terminology of Daganzo *et al.* [62], the perturbation will eventually "activate the bottleneck" associated with the on-ramp. In the following, we will explain and quantify the mechanism of this transition.

According to Figure 10, the perturbation triggers a stop-and-go wave, which travels downstream as long as it is small and upstream as it becomes larger, as is known from "localized clusters" [58]. Now, assume the downstream front of the cluster would pass the on-ramp. Then, since Q_{main} (Figure 10c) is lower than the characteristic outflow Q_{out} from a jam, the cluster would eventually vanish. However, during its lifetime, the cluster would continue to emit the flow Q_{out}, leading downstream of the ramp to a flow $Q_{\mathrm{out}} + Q_{\mathrm{rmp}}/n > Q_{\mathrm{max}}$. As a consequence, as soon as the perturbation reaches the on-ramp, it induces congested traffic with a *standing* downstream front just at the end of the ramp. With an observed outflow $\tilde{Q}_{\mathrm{out}} \leq Q_{\mathrm{out}}$ from synchronized traffic (with $\tilde{Q}_{\mathrm{out}} \approx Q_{\mathrm{out}}$), the average flow upstream is given by

$$Q_{\mathrm{sync}} = \tilde{Q}_{\mathrm{out}} - \frac{Q_{\mathrm{rmp}}}{n}. \tag{27}$$

Hence, the congested region upstream of the on-ramp is growing until the flow Q_{main} from the main road drops below Q_{sync}. Only then the congested region starts to "melt", and it can easily take an additional hour or so until traffic returns to free flow, even if the maximum flow Q_{max} has never been exceeded by $(Q_{\mathrm{main}} + Q_{\mathrm{rmp}}/n)$!

Now, consider the density ρ_{sync} defined by $Q_{\mathrm{sync}} = Q_{\mathrm{e}}(\rho_{\mathrm{sync}})$ in the congested part of the equilibrium flow-density relation $Q_{\mathrm{e}}(\rho)$ (i.e., behind its maximum). If homogeneous traffic is (meta-)stable at ρ_{sync}, the on-ramp induces "synchronized" congested traffic. The restriction

$Q_{\mathrm{rmp}} \leq \tilde{Q}_{\mathrm{out}}/2$ [63] implies $Q_{\mathrm{sync}} \geq \tilde{Q}_{\mathrm{out}}(1 - 1/2n)$ and $\rho_{\mathrm{sync}} < \rho_{\mathrm{jam}}$, so that "synchronized" congested flow is significantly higher than the flow inside traffic jams.

2.6. Phase Diagram of Traffic States at Bottlenecks

Close to bottlenecks by on-ramps, lane closures, gradients, or other effects (including building sites along the road, bad street conditions, restricted visibility, curves, accidents in the opposite lanes, and slow vehicles), there can develop a variety of different traffic states. Free traffic (FT) and the above-discussed type of "synchronized" congested traffic, which we will also call "homo-

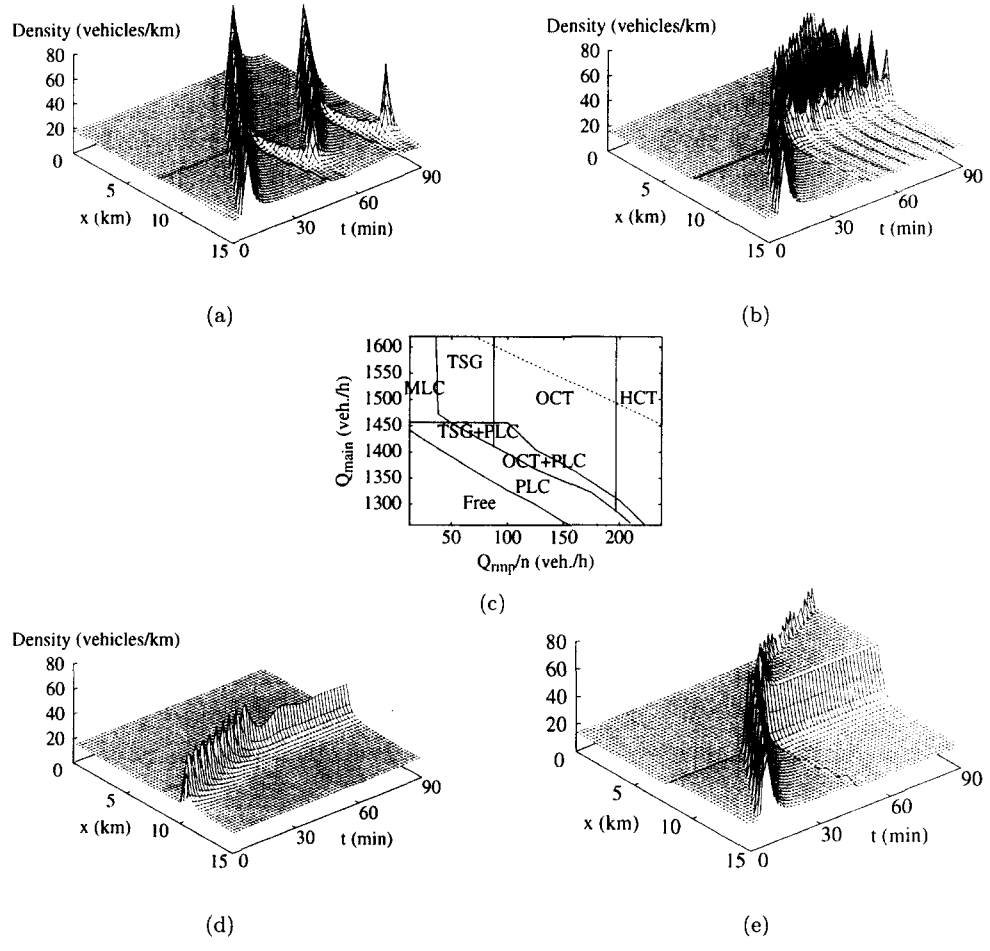

Figure 11. (a),(b),(d), and (e): Spatiotemporal dynamics of typical representatives of congested states which are triggered at an on-ramp by a fully developed perturbation travelling upstream. The middle of the on-ramp is located at $x = 8.0\,\mathrm{km}$. The respective states are (a) triggered stop-and-go traffic (TSG) for $Q_{\mathrm{main}} = 1660$ vehicles/h/lane and $Q_{\mathrm{rmp}}/n = 75$ vehicles/h, (b) oscillatory congested traffic (OCT) for $Q_{\mathrm{main}} = 1540$ vehicles/h/lane and $Q_{\mathrm{rmp}}/n = 170$ vehicles/h, (d) a pinned localized cluster (PLC) for $Q_{\mathrm{main}} = 1450$ vehicles/h/lane and $Q_{\mathrm{rmp}}/n = 60$ vehicles/h, and (e) homogeneous congested traffic (HCT) for $Q_{\mathrm{main}} = 1350$ vehicles/h/lane and $Q_{\mathrm{rmp}}/n = 400$ vehicles/h. The other model parameters used in the above simulations are $V_0 = 110\,\mathrm{km/h}$, $\rho_{\mathrm{max}} = 140\,\mathrm{Fz/km}$, $\tau = 40\,\mathrm{s}$, $T = 1.7\,\mathrm{s}$, $\gamma = 1.2$, $A_0 = 0.008$, $\Delta A = 0.02$, $\rho_c = 0.27\rho_{\mathrm{max}}$, $\Delta\rho = 0.1\rho_{\mathrm{max}}$, and $L = 400\,\mathrm{m}$. They can be considered as typical for German freeways, where all the above congested traffic states have been empirically observed. (c) Corresponding phase diagram of the traffic states forming in the vicinity of an on-ramp as a function of the inflows Q_{main} and Q_{rmp}/n per freeway lane on the main road and the on-ramp for the above parameters. The different states are classified at $t = 90\,\mathrm{min}$, i.e., after a sufficiently long transient period. Displayed are homogeneous congested traffic (HCT), oscillatory congested traffic (OCT), triggered stop-and-go traffic (TSG), moving localized clusters (MLC), pinned localized clusters (PLC), and free traffic (FT). Spatially coexisting states are indicated with a plus sign. The broken line represents the condition $Q_{\mathrm{main}} + Q_{\mathrm{rmp}}/n = Q_{\mathrm{max}}$ that separates the region in which a breakdown of traffic flow is caused by exceeding the theoretically possible freeway capacity Q_{max} (upper right corner). Note that all congested traffic states below this line are caused by perturbations and, therefore, avoidable by technical control measures.

geneous congested traffic" (HCT), are only two of them. Other congested traffic states that can emerge are "oscillating congested traffic" (OCT), "triggered stop-and-go waves" (TSG), "moving localized clusters" (MLC), and "pinned (standing) localized clusters" (PLC) (see Figure 11). All these different congested states are observable in empirical traffic data [5,11,13,18,54,62], although the "synchronized" congested states have sometimes been interpreted differently in the beginning.

In our traffic simulations, we found out that most of the congested traffic states occur below the capacity limit $Q_{\max}$, and they are triggered by perturbations in traffic flow. This is only possible since the outflow Q_{out} from traffic jams is an additional, self-organized capacity limit, which is smaller than $Q_{\max}$ (due to the larger time headways occuring in accelerating traffic). The same fact brings about that most breakdowns of traffic flow could be avoided by control measures which manage to suppress these perturbations.

Our simulations also indicate that the conditions, under which the different traffic states appear, are clearly defined [22,65]. This is illustrated by the phase diagram in Figure 11c, displaying the traffic states as a function of the main flow Q_{main} and the on-ramp flow per freeway lane, Q_{rmp}/n (which is a measure of the flow reduction by a bottleneck). It explains why usually not all possible congested traffic states are observed at every bottleneck, but only a typical, site-specific subset of them. The phase diagram also allows us to understand the various observed transitions between the traffic states, which correspond to crossing the phase boundaries separating the different states. Notice that these phase boundaries can be calculated analytically in terms of the flows $Q_{ci} = Q_e(\rho_{ci})$ characterizing the stability diagram (see Section 2.2). This implies that the general structure of the phase diagram in Figure 11c is expected to be *universal* for all microscopic and macroscopic traffic models which possess the same instability diagram (i.e., the sequence of stable, metastable, unstable, convectively stable, metastable, and stable traffic with increasing density). Only the exact position and the shape of the phase boundaries will vary from one model to another.

Multistability and spatial coexistence of states

Note that the phase diagram in Figure 11c is for fully developed perturbations. For smaller perturbations, the phase boundaries will be shifted. The MLC and PLC regimes may even disappear, leading to the boundaries FT $\leftrightarrow$ TSG, FT $\leftrightarrow$ OCT, and FT $\leftrightarrow$ HCT. In any case, there are regions of multistability, where the resulting traffic state depends on the initial condition. Similar to Lee *et al.* [66], we could even find a small region of tristable traffic (TRI), where we can have FT, PLC, or OCT, depending on the respective "history" of the traffic dynamics. Figure 12a shows, for example, a transition from PLC to OCT.

Another interesting point is the possible spatial coexistence of different traffic states. If congested traffic is linearly unstable, but convectively stable, upstream of a bottleneck we can have the following sequences of states, depending on the model parameters and the length of the congested region.

(i) Empirical data and simulation results of the sequence HCT $\rightarrow$ OCT (without mergers of small density oscillations to fully developed stop-and-go waves) are presented in [67].

(ii) The sequence HCT $\rightarrow$ OCT $\rightarrow$ TSG (see Figure 12b) is discussed in [21] (for a slightly modified GKT model with frustration effects), and we think that it can explain the empirically observed sequence "synchronized" traffic $\rightarrow$ "pinch region" $\rightarrow$ stop-and-go waves reported in [19].

In Section 3.7, we will come back to the subjects of this paragraph.

Qualitative interpretation of the transitions

Finally, we give a qualitative interpretation of the transitions between the various congested traffic states and the respective conditions under which they appear. For example, the transition

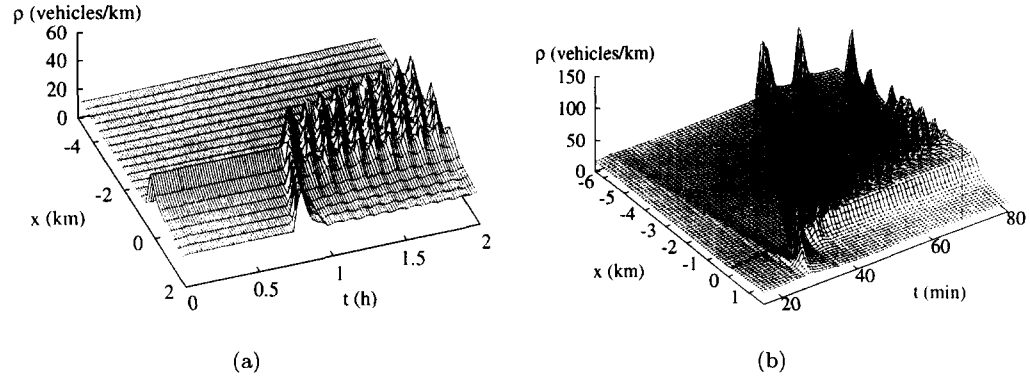

(a) (b)

Figure 12. (a) Metastable pinned localized cluster (PLC) and stable oscillating congested traffic (OCT), simulated with the nonlocal GKT model (with model parameters $v_0 = 120\,\text{km/h}$, $T = 1.8\,\text{s}$, $\tau = 50\,\text{s}$, $\rho_{\max} = 130$ vehicles/km, $\gamma = 1.2$, $A_0 = 0.008$, and $\Delta A = 0.008$). The inflow to the main road is 1400 vehicles per hour and lane, and the assumed inhomogeneity of traffic flow comes from an on-ramp of length 500 m with a constant inflow of 140 vehicles per hour and lane. The metastable PLC is triggered by a triangular-shaped density peak in the initial conditions (of total width 500 m, centered at $x = 0$), in which the density rises from 14 vehicles/km to 40 vehicles/km. The OCT is triggered by a density wave introduced by the downstream boundary conditions. (b) Spatiotemporal evolution of the traffic density according to the gas-kinetic-based traffic model [20]. The assumed inhomogeneity of traffic flow comes from an on-ramp of length 200 m with an inflow of 220 vehicles per hour and freeway lane. The inflow to the main road is 1570 vehicles per hour and lane, and the breakdown of traffic flow is triggered by a perturbation $\Delta Q(t)$ of the inflow with a flow peak of 125 vehicles per hour and lane (see main text). The assumed model parameters are $V_0 = 120\,\text{km/h}$, $T = 1.5\,\text{s}$, $\tau = 30\,\text{s}$, $\rho_{\max} = 120$ vehicles/km, and $\gamma = 1.2$, while the parameters for the variance prefactor [20] $A(\rho) = A_0 + \Delta A\{\tanh[(\rho - \rho_c)/\Delta\rho] + 1\}$ are $A_0 = 0.008$, $\Delta A = 0.02$, $\rho_c = 0.27\rho_{\max}$, and $\Delta\rho = 0.1\rho_{\max}$. In order to have a large region of linearly unstable but convectively stable traffic, we introduced a "resignation effect", i.e., a density-dependent reduction of the desired velocity V_0 to $V_0'(\rho) = V_0 - \Delta V/\{1 + \exp[(\rho_c' - \rho)/\Delta\rho']\}$ with $\Delta V = 0.9V_0$, $\rho_c' = 0.45\rho_{\max}$, and $\Delta\rho = 0.1\rho_{\max}$.

HCT $\rightarrow$ OCT from homogeneous to oscillating congested traffic occurs when the ramp flow Q_{rmp} is decreased so that the synchronized flow (27) falls into the unstable density regime instead of the (meta-)stable one. A further decrease in the ramp flow will reduce the average density in the congested region so much that we will have an alternation between regimes of free and congested traffic, which defines stop-and-go waves. We call them triggered stop-and-go waves (TSG) because whenever an upstream travelling jam passes the bottleneck, it triggers a small perturbation which travels downstream as long as it is small, but eventually changes its speed as it grows and changes its propagation direction. Finally, the developed perturbation travels upstream and passes the bottleneck, where it gives birth to a new perturbation, and so on.

Obviously, the small triggered perturbation cannot grow when the traffic flow downstream of the bottleneck is (meta-)stable, which will lead to a single localized cluster (LC). The localized cluster will pass the bottleneck in upstream direction (MLC), if traffic flow is unstable or metastable there. In contrast, the localized cluster will be pinned at the bottleneck (PLC) if traffic in the upstream region is stable since a density cluster could not survive there. If the traffic flow downstream of the bottleneck is also stable, only free traffic (FT) can persist. Finally, the pinned localized cluster will grow to an extended region of congested traffic, if its outflow $\tilde{Q}_{\text{out}}$ is smaller than the total flow $(Q_{\text{main}} + Q_{\text{rmp}}/n)$ at the bottleneck.

Discussion

Although there are also other proposals for an explanation of the various transitions between free traffic, congested traffic, and stop-and-go waves [19], we see the following advantages of our approach. The transitions result *naturally* from a model for traffic flow on *homogeneous* roads, just by adding source terms (in case of on-ramp flows) [22] or other kinds of inhomogeneities like speed limits (see Section 3.7), which are *known* to exist. The implementation of these inhomogeneities is *straightforward* without the requirement of additional refined model ingredients.

Moreover, analogous to the other parameters of the model, the inhomogeneities are easily measurable quantities. There is no model ingredient which could not be relatively easily verified or falsified by empirical studies. Furthermore, *empirical results* confirming the existence of a phase diagram are already available [16,67]. Finally, we think that the simulated traffic states related to inhomogeneities of the road arise *so* naturally that any explanation of empirical data must take these states into account.

2.7. Velocity Correlations of Successive Cars

With a few exceptions only (see, e.g., [44,46]), Boltzmann-like traffic equations are evaluated with the assumption of "vehicular chaos", which neglects correlations r between the velocities of successive vehicles. This is also true for the results presented above, mainly because empirical data of the correlation coefficient r have not been available until very recently (see Figure 13). As expected, the velocity correlations are small for low vehicle densities, but considerable in congested traffic. Fortunately, it is possible to generalize the above nonlocal, gas-kinetic-based traffic model in a way that allows us to take the velocity correlations into account [53,68]. It turns out that one has only to replace formula (9) by

$$S = \theta - 2r\sqrt{\theta\theta'} + \theta'. \tag{28}$$

Obviously, this mainly modifies the equilibrium velocity a bit, similar to a reduction of velocity variances. Therefore, we expect only quantitative, but no qualitative (fundamental) changes in the simulation results for finite values of r.

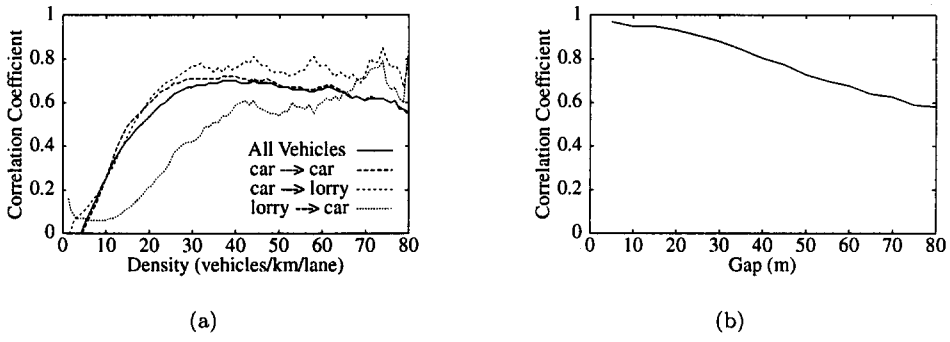

Figure 13. Correlation between the velocity of successive vehicles (a) in the right lane as a function of the density (b) as a function of the gap between successive vehicles for a density of 10 vehicles per kilometer. The relations were determined from single-vehicle data from the Dutch freeway A9. According to our empirical results, the correlation coefficient is about zero at small densities and reaches a maximum at around 20 to 30 vehicles per kilometer, where the transition from free to congested traffic occurs. Afterwards, it stays on a high level (around 0.65). In the left lane, the velocity correlation is a little bit higher, probably because of the smaller fraction of lorries. The correlation coefficient is not sensitive to the type of the leading vehicle (car or lorry), but to that of the following vehicle, which is reasonable. However, even at small densities, the correlation depends strongly on the gap to the next vehicle ahead and becomes almost one for very small gaps. This is because different velocities would imply a high danger of accidents then.

3. CAR-FOLLOWING MODELS

For about 50 years now, researchers have modelled freeway traffic by means of continuous-in-time microscopic models (car-following models) [69]. Since then, a multitude of car-following models have been proposed, both for single-lane and multilane traffic including lane changes.

In the simplest case, the acceleration of an individual vehicle depends only on the distance to the vehicle in front. Well-known models of this type include the model by Newell [70], or the "optimal-velocity model" by Bando *et al.* [71]. To achieve a better anticipative driver behavior and to avoid collisions, the acceleration in other models depends also on the velocity and on

the approaching rate to the front vehicle [72–74]. Besides these simple models intended for basic investigations, there are also highly complex "high-fidelity models" like the Wiedemann model [75] or MITSIM [76]. They try to reproduce traffic as realistically as possible, but at the cost of plenty of parameters, which are difficult to calibrate.

In the following, we will propose and discuss a novel follow-the-leader model that contains a few parameters only, all of which have a reasonable interpretation, are known to be relevant, are empirically measurable, and have the expected order of magnitude. The fundamental diagram and the stability properties of the model can be easily (and separately) calibrated to empirical data, and simulations of all kinds of observed traffic breakdowns are possible with the measured boundary conditions [67]! Moreover, an equivalent macroscopic version of the model is known, which is not the case for most other microscopic traffic models. Finally, we mention that the new model behaves accident-free because of the dependence on the relative velocity. For similar reasons and because of metastability, it shows the self-organized characteristic traffic constants mentioned before.

3.1. The Microscopic Intelligent-Driver Model (IDM)

The acceleration assumed in the IDM is a continuous function of the velocity v_α, the (netto) gap s_α, and the velocity difference (approaching rate) Δv_α of vehicle α to the leading vehicle:

$$\dot{v}_\alpha = a^{(\alpha)} \left[1 - \left(\frac{v_\alpha}{v_0^{(\alpha)}} \right)^\delta - \left(\frac{s_\alpha^*(v_\alpha, \Delta v_\alpha)}{s_\alpha} \right)^2 \right] . \tag{29}$$

This expression is a superposition of the acceleration $a^{(\alpha)}[1 - (v_\alpha/v_0^{(\alpha)})^\delta]$ on a free road, and a braking deceleration $-a^{(\alpha)}[s_\alpha^*(v_\alpha, \Delta v_\alpha)/s_\alpha]^2$, describing the interactions with other vehicles. The deceleration term depends on the ratio between the "desired gap" s_α^* and the actual gap s_α, where the desired gap

$$s_\alpha^*(v, \Delta v) = s_0^{(\alpha)} + s_1^{(\alpha)} \sqrt{\frac{v}{v_0^{(\alpha)}}} + T_\alpha v + \frac{v \Delta v}{2\sqrt{a^{(\alpha)} b^{(\alpha)}}} \tag{30}$$

is dynamically varying with the velocity and the approaching rate, reflecting an intelligent driver behavior. The IDM parameters are the desired velocity v_0, safe time headway T, maximum acceleration a, comfortable deceleration b, acceleration exponent δ, and the jam distances s_0 and s_1. Furthermore, the vehicles have a finite length l which, however, has no dynamical influence. In Sections 3.1 to 3.7, we will assume identical "cars", while in Section 3.8, we assume two different types, "cars" and "lorries"; see Table 2. For better readability, we will drop the vehicle index α in the following discussion of the model.

Table 2. Model parameters of the IDM model used throughout this paper.

Type	v_0	T	a	b	s_0	s_1	l
Cars	120 km/h	1.2 s	0.8 m/s^2	1.25 m/s^2	1 m	10 m	5 m
Lorries	80 km/h	1.7 s	0.4 m/s^2	0.8 m/s^2	1 m	10 m	8 m

3.2. Equilibrium Traffic of Identical Vehicles

In equilibrium traffic ($\dot{v}_\alpha = 0$, $\Delta v_\alpha = 0$), drivers tend to keep a velocity-dependent equilibrium gap $s_e(v_\alpha)$ to the front vehicle given by

$$s_e(v) = s^*(v, 0) \left[1 - \left(\frac{v}{v_0} \right)^\delta \right]^{-1/2} . \tag{31}$$

In particular, the equilibrium gap of homogeneous *congested* traffic ($v \ll v_0$) is essentially equal to the desired gap, $s_e(v) \approx s^*(v,0) = s_0 + s_1\sqrt{v/v_0} + vT$; i.e., it is composed of a (small) high-density contribution, and a contribution vT corresponding to a time headway T.

Solving equation (31) for the equilibrium velocity $v = v_e$ leads to simple expressions only for $s_1 = 0$ and $\delta = 1$, $\delta = 2$, or $\delta \to \infty$. In particular, the equilibrium velocity for the special case $\delta = 1$ and $s_0 = s_1 = 0$ is

$$v_e(s) = \frac{s^2}{2v_0T^2}\left(-1 + \sqrt{1 + \frac{4T^2v_0^2}{s^2}}\right). \tag{32}$$

Macroscopically, homogeneous traffic consisting of identical vehicles can be characterized by the equilibrium traffic flow $Q_e(\rho) = \rho V_e(\rho)$ as a function of the traffic density ρ. For $\delta = 1$ and $s_0 = s_1 = 0$, this "fundamental diagram" follows from equation (32) together with the micro-macro relation between gap and density

$$s = \frac{1}{\rho} - l = \frac{1}{\rho} - \frac{1}{\rho_{\max}}. \tag{33}$$

The resulting relation for the density-dependent equilibrium velocity is identical to that of the GKT model, if the GKT parameter ΔA is set to zero (see equations (19) and (20)), which is a necessary condition for a micro-macro correspondence. Figure 14a shows that the acceleration coefficient δ influences the transition region between the free and congested regimes. For $\delta \to \infty$ and $s_1 = 0$, the fundamental diagram becomes triangular-shaped: $Q_e(\rho) = \min(v_0\rho, [1 - \rho(l + s_0)]/T)$. For decreasing δ, it becomes smoother and smoother.

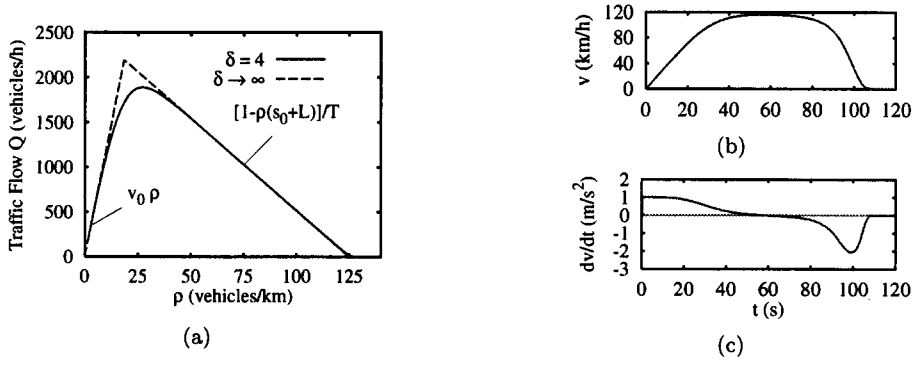

Figure 14. (a) Equilibrium flow-density diagram of identical IDM vehicles with variable acceleration exponent δ and the "car" parameters of Table 2 otherwise. (b),(c) Temporal evolution of the velocity and acceleration of a single vehicle approaching a standing obstacle, which is reached after $t = 106\,\mathrm{s}$ (cf., main text). The IDM parameters are $a = 1\,\mathrm{m/s^2}$, $b = 2\,\mathrm{m/s^2}$, and the "car" parameters of Table 2 otherwise.

3.3. Dynamic Single-Vehicle Properties

Figures 14b and 14c show how the parameters a and b determine the acceleration and braking behavior of single vehicles. At $t = 0$, one vehicle starts with zero velocity and 2.5 km of free road ahead. Initially, it accelerates with a and approaches smoothly the desired velocity v_0. At $x = 2.5\,\mathrm{km}$, we assume a standing obstacle, for example, the end of a traffic jam. When approaching the obstacle, the model mimics "intelligent" drivers who anticipate necessary braking decelerations and brake so as not to exceed the comfortable deceleration b in normal situations [21].

3.4. Calibration

The *fundamental relations* of homogeneous traffic are calibrated with v_0 (low density), δ (transition region), T (high density), and s_0 and s_1 (jammed traffic). The *stability behavior* of traffic

in the IDM model is determined mainly by the model parameters a, b, and T. The density in and the outflow from traffic jams are also influenced by s_0 and s_1. Since the accelerations a and b do not influence the fundamental diagram, the model can be calibrated essentially independently with respect to traffic flows and stability. As in the GKT model, traffic becomes more unstable for decreasing a (which corresponds to an increased acceleration time $\tau = v_0/a$), and for decreasing T (corresponding to reduced safe time headways). Furthermore, the instability increases with growing b. This is also plausible, because an increased desired deceleration b corresponds to a less anticipative braking behavior.

3.5. Collective Behavior and Stability Diagram

Although we are interested in realistic *open* systems, it turned out that many features can be explained in terms of the stability behavior in a *closed* system. Figure 15a shows the stability diagram of homogeneous traffic on a circular road. The control parameter is the homogeneous (average) density $\bar{\rho}$. We applied both a very small and a large localized perturbation to check for linear and nonlinear stability, and plotted the resulting minimum (ρ_{out}) and maximum (ρ_{jam}) densities after a stationary situation was reached. The resulting diagram is very similar to that of the macroscopic KKKL and GKT models [10,20]. In particular, it displays the following realistic features.

(i) Traffic is stable for very low and high densities, but unstable for intermediate densities.

(ii) There is a density range $\rho_{c1} \leq \bar{\rho} \leq \rho_{c2}$ of metastability; i.e., only perturbations of sufficiently large amplitudes grow, while smaller perturbations disappear. Note that for most IDM parameter sets, there is no second metastable range at higher densities, in contrast to the GKT and KKKL models.

(iii) The density inside of traffic jams and the associated flow $Q_{\text{jam}} = Q_e(\rho_{\text{jam}})$, cf., Figure 15b, do not depend on $\bar{\rho}$.

As further "traffic constants", at least in the density range 20 veh./km $\leq \bar{\rho} \leq$ 40 veh./km, we observe a constant outflow $Q_{\text{out}} = Q_e(\rho_{\text{out}})$ and propagation velocity $v_g = (Q_{\text{out}} - Q_{\text{jam}})/(\rho_{\text{out}} - \rho_{\text{jam}}) \approx -15$ km/h of jams. Figure 15b shows the stability diagram for the flows. In particular, we have $Q_{c1} < Q_{\text{out}} < Q_{c2}$, where $Q_{ci} = Q_e(\rho_{ci})$; i.e., the outflow from congested traffic is metastable, while in the GKT, $Q_{\text{out}} \approx Q_{c2}$ is only marginally stable.

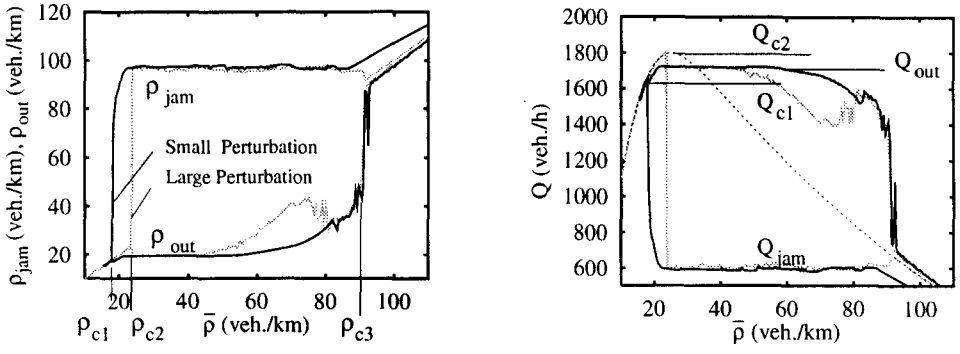

Figure 15. Stability diagram of homogeneous traffic (for "car" parameters) in a closed system as a function of the homogeneous density $\bar{\rho}$ for small (grey) and large (black) initial perturbations of the density. In plot (a), the upper two lines display the density inside of density clusters after a stationary state has been reached. The lower two lines represent the density between the clusters. Plot (b) shows the corresponding flows and the equilibrium flow-density relation (dotted). The critical densities ρ_{ci} and flows Q_{ci} are discussed in the main text.

In *open* systems, a third type of stability becomes relevant. Traffic is *convectively* stable if, after a sufficiently long time, all perturbations are convected out of the system. Both in the

macroscopic models and in the IDM, there is a considerable density region $\rho_{cv} \leq \bar{\rho} \leq \rho_{c3}$, where traffic is linearly unstable but convectively stable.

3.6. Microscopic Implementation of Bottlenecks

In *macroscopic* simulations, a natural implementation of road inhomogeneities is given by on- and off-ramps, which appear as a source term in the continuity equation for the density. An explicit *microscopic* modelling of ramps, however, would require a multilane model with explicit simulation of lane changes. In order to avoid the associated complications, one can either apply the micro-macro link and simulate the ramp section macroscopically (see Section 4), or introduce *flow-conserving* inhomogeneities by making one or more model parameters dependent on the location x of the road. Suitable parameters for the IDM are v_0 or T [21,67]. Local parameter variations act as a bottleneck, if the outflow Q'_{out} from congested traffic in the downstream section is reduced with respect to the outflow Q_{out} in the upstream section. This requires a reduced desired velocity $v'_0 < v_0$ or increased time headway $T' > T$, or both. Figure 16a shows a traffic breakdown induced by a linear decrease of the desired velocity from $v_0 = 120\,\text{km/h}$ for $x \leq -L/2$ to $v'_0 = 95\,\text{km/h}$ for $x \geq L/2$, while Figure 16c shows the same effect for an increase of the safe time headway from $T = 1.2\,\text{s}$ to $T' = 1.45\,\text{s}$ ($L = 200\,\text{m}$). Both flow-conserving bottlenecks result in a similar traffic dynamics which, however, depends strongly on the amplitude of the parameter variation. Qualitatively, the same dynamics is observed in real traffic data (Figure 16e) and in macroscopic models including on-ramps with a ramp flow of $Q_{\text{rmp}}/n = (Q_{\text{out}} - Q'_{\text{out}})$.

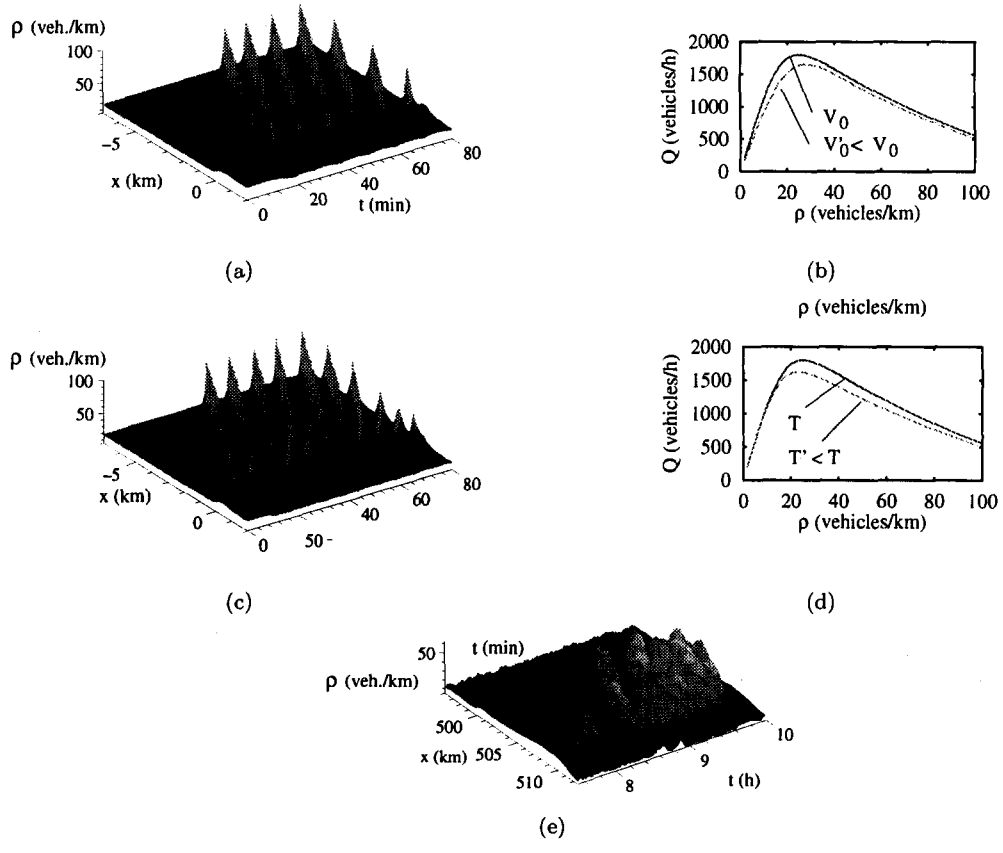

Figure 16. Traffic breakdowns at differently implemented bottlenecks. (a) IDM simulation of the spatiotemporal density (inflow $Q_{\text{main}} = 1670$ vehicles/h) for a bottleneck corresponding to a decrease of v_0 in the downstream region. The density is derived from the microscopic distance s via relation (33) and a subsequent linear interpolation. (b) Related equilibrium flows upstream and downstream. (c),(d) Bottleneck corresponding to an increase of the safe time headway T. (e) Density obtained from one-min detector data of the German freeway A9-South on October 29, 1998. The traffic breakdown takes place upstream of the intersection "Neufahrn" at $x = 512\,\text{km}$.

This suggests that we define a general "bottleneck strength" ΔQ by

$$\Delta Q := \frac{Q_{\text{rmp}}}{n} + Q_{\text{out}} - Q'_{\text{out}}. \tag{34}$$

In particular, we have $\Delta Q = Q_{\text{rmp}}/n$ for on-ramp bottlenecks, and $\Delta Q = Q_{\text{out}} - Q'_{\text{out}}$ for flow-conserving bottlenecks. In the following, we will vary v_0. The regions with locally decreased desired velocity can be interpreted as sections with uphill gradients (which reduce the maximum velocities of vehicles).

3.7. Phase Diagram of Congested Traffic

In contrast to *closed* systems, in which the long-term behavior and stability is essentially determined by the average traffic density, the dynamics of *open* systems is controlled by the inflow Q_{main}. Furthermore, traffic congestions depend on road inhomogeneities and, because of hysteresis effects, on the history of previous perturbations. For a given history, the traffic states can be summarized by a phase diagram spanned by Q_{main} and ΔQ. Figure 17 shows the IDM phase diagram for traffic states that develop after a single density cluster crosses the inhomogeneity. Depending on Q_{main} and ΔQ, the initial perturbation

(i) dissipates, resulting in free traffic (FT),

(ii) travels through the inhomogeneity as a moving localized cluster (MLC) and neither dissipates nor triggers new breakdowns,

(iii) triggers a traffic breakdown to a pinned localized cluster (PLC), which remains localized near the inhomogeneity for all times and either is stationary, cf., Figure 18a for $t < 0.2$ h, or oscillatory (OPLC).

(iv) Finally, the initial perturbation can induce extended congested traffic (CT), whose downstream boundaries are fixed at the inhomogeneity, while the upstream front propagates further upstream in the course of time.

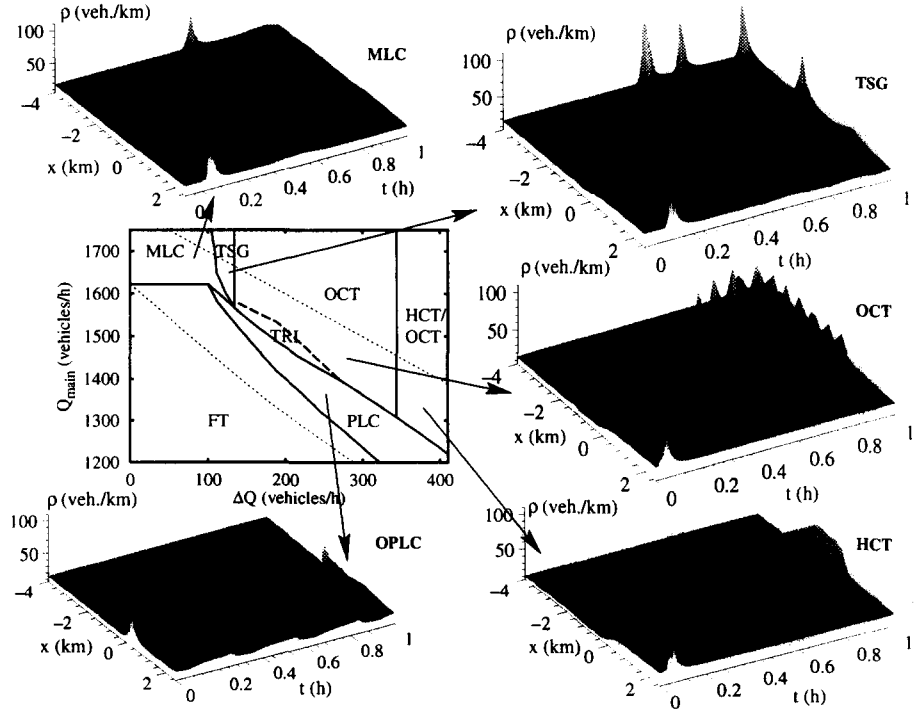

Figure 17. Phase diagram of congested traffic states and corresponding spatiotemporal density plots as simulated with the IDM. The control parameters are the inflow Q_{main} and the bottleneck strength ΔQ, which increases with $(v_0 - v'_0)$. The traffic states FT, HCT, OCT, TSG, MLC, and (O)PLC are explained in the main text. "TRI" indicates a tristable region.

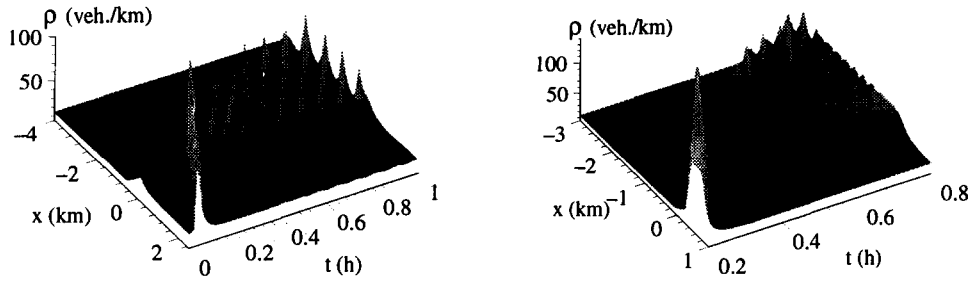

(a) (b)

Figure 18. (a) Transition from a pinned localized cluster (PLC) to oscillating congested traffic (OCT) in the tristable region ($Q_{\text{main}} = 1480$ vehicles/h, $v_0' = 24$ m/s corresponding to $\Delta Q = 220$ vehicles/h), triggered by a large perturbation. (b) Spatial coexistence of HCT and OCT for $Q_{\text{main}} = 1350$ vehicles/h and $v_0' = 16$ m/s corresponding to $\Delta Q = 400$ vehicles/h.

This kind of congested traffic can be homogeneous (HCT), oscillatory (OCT), or consist of triggered stop-and-go waves (TSG). The observed traffic states and their qualitative dependence on Q_{main} and ΔQ is the same as for the GKT model, Figure 11 when identifying ΔQ with Q_{rmp}/n according to equation (34). In contrast to OCT, where there is permanently congested traffic at the inhomogeneity ("pinch region" [19,21]), the TSG state is characterized by a series of isolated density clusters, each of which triggers a new cluster as it passes the inhomogeneity.

Boundaries between and coexistence of traffic states

Simulations show that the outflow $\tilde{Q}_{\text{out}}$ from the nearly stationary downstream fronts of OCT and HCT satisfies $\tilde{Q}_{\text{out}} \leq Q'_{\text{out}}$, where Q'_{out} is the outflow from clusters in homogeneous systems for the downstream model parameters. If the bottleneck is not too strong, we have $\tilde{Q}_{\text{out}} \approx Q'_{\text{out}}$. Then, for all types of bottlenecks, the congested traffic flow is given by $Q_{\text{cong}} = \tilde{Q}_{\text{out}} - Q_{\text{rmp}}/n \approx Q'_{\text{out}} - Q_{\text{rmp}}/n$, or

$$Q_{\text{cong}} \approx Q_{\text{out}} - \Delta Q, \tag{35}$$

which generalizes (27). Extended congested traffic (CT) only persists if the inflow exceeds the congested traffic flow. Otherwise, it dissolves to PLC. This gives the boundary

$$\text{CT} \rightarrow \text{PLC} : \Delta Q \approx Q_{\text{out}} - Q_{\text{main}}. \tag{36}$$

If congested traffic flow is *convectively* unstable, the resulting oscillations lead to TSG or OCT. If it is *linearly* stable, $Q_{\text{cong}} < Q_{\text{c3}}$, we have HCT. If it is convectively stable, but linearly unstable, $Q_{\text{cong}} \in [Q_{\text{c3}}, Q_{\text{cv}}]$, one has a spatial *coexistence* of states with HCT near the bottleneck and OCT further upstream [21] (Figure 18), which is frequently found in empirical data of congested traffic. In the IDM, this frequent occurrence is reflected by the wide range of flows falling into this regime. For the "car" parameters, we have $Q_{\text{c3}} = 600$ vehicles/h and $Q_{\text{cv}} = 1340$ vehicles/h.

Pinch effect and merging of clusters

Careful investigations of traffic data related to OCT states [19] showed two phenomena.

(i) In a narrow region near the inhomogeneity, congested traffic is nearly stationary ("pinch region"), while further upstream, there are oscillations of the traffic density.

(ii) While propagating upstream, the oscillations grow and merge to a few large-amplitude density clusters with free traffic in between. Detector data of other freeways, however, show a pinch effect without mergers, cf., Figure 16e.

Simulating the IDM with the "car" parameters leads to very few mergers; cf., Figures 16c and 17. For other parameters, however, the IDM reproduces mergers ending up with stop-and-go traffic [21]. A possible explanation is the *"starvation effect"*: for the parameters chosen in this article,

the outflow Q_{out} from density clusters is in the middle of the metastable region (Figure 15b), so medium-sized and large density clusters persist. For the parameters of [21], however, the outflow from density clusters satisfies $Q_{\text{out}} \approx Q_{\text{c1}}$, so only large-amplitude clusters survive, while all others dissipate.

Multistability

In general, the local phase transitions between free traffic, pinned localized states, and extended congested states are hysteretic. In the regions between the two dotted lines of the phase diagram in Figure 17, both free and congested traffic are possible, depending on the previous history. In particular, for all five indicated phase points (but not for the simulations of Figure 16), free traffic would persist without the downstream perturbation. In contrast, the transitions PLC $\longrightarrow$ OPLC, and HCT $\longrightarrow$ OCT $\longrightarrow$ TSG seem to be nonhysteretic; i.e., the type of pinned localized cluster or of extended congested traffic is uniquely determined by Q_{main} and ΔQ.

In a small subset of the metastable region labelled "TRI" in Figure 17, we even found *tristability* between FT, PLC, and OCT. We obtained qualitatively the same also for the GKT model, and it has been found for the KKKL model with OPLC instead of PLC for the pinned localized state [34]. Figure 18a shows that a single moving localized cluster passing the inhomogeneity triggers a transition from PLC to OCT. Starting with free traffic, the same perturbation would trigger OCT as well, while we never found reverse transitions OCT $\rightarrow$ PLC or OCT $\rightarrow$ FT (without a reduction of the inflow). That is, FT and PLC are metastable in the tristable region, while OCT is stable.

3.8. Multispecies Single-Lane Traffic

In this section, we assume heterogeneous single-lane traffic consisting of 70% "cars" and 30% "lorries", where the latter are characterized by a lower desired velocity, lower accelerations, and a larger safe time headway compared to cars (Table 2). Again, we simulate a traffic breakdown to HCT at a flow-conserving inhomogeneity, where the desired velocity of cars is reduced from 120 km/h to 65 km/h, and that of lorries from 80 km/h to 36 km/h. (Similar results are found for less dramatic increases of T.) To compare the result with real traffic data, we implement "virtual" detectors at several fixed locations. The detectors record passage times and velocities of each vehicle to determine the macroscopic flow $Q = n_\tau/\tau$ (where n_τ is the number of passing vehicles in the averaging interval $\tau = 45$ s), the arithmetic velocity average V, and the density $\rho = Q/V$. Figure 19 shows the resulting fundamental diagram 3 km upstream of the bottleneck, and time series of Q and V at three upstream locations. For comparison, Figures 19d and 19e show 45 s averages of *real* single-vehicle data of the Dutch freeway A9 from Haarlem to Amsterdam on October 14, 1994. The detector is about 0.7 km upstream of the on-ramp causing the traffic breakdown. The simulated and real traffic data agree qualitatively, in particular in the following respects.

(i) There is a wide scattering of flow-density data in the congested regime (looking like an anisotropic two-dimensional random walk), while the data occupy a nearly one-dimensional region in the free regime.

(ii) The distribution of flow-density data shows the typical inverse-λ form with a distinct gap between free and congested traffic data.

(iii) During the breakdown, the velocity drops to 10–20 km/h, while the flow is reduced by only about 20%.

(iv) In all regions, the relative fluctuations of the velocity are smaller than those of the flow. Near the bottleneck, the fluctuations of congested traffic flow are much smaller than those of free traffic, while further upstream, the fluctuations grow.

Notice that the fluctuations of the simulated data come essentially from the different vehicle types and not from deterministic instabilities. Macroscopically, the situation of Figure 19 corre-

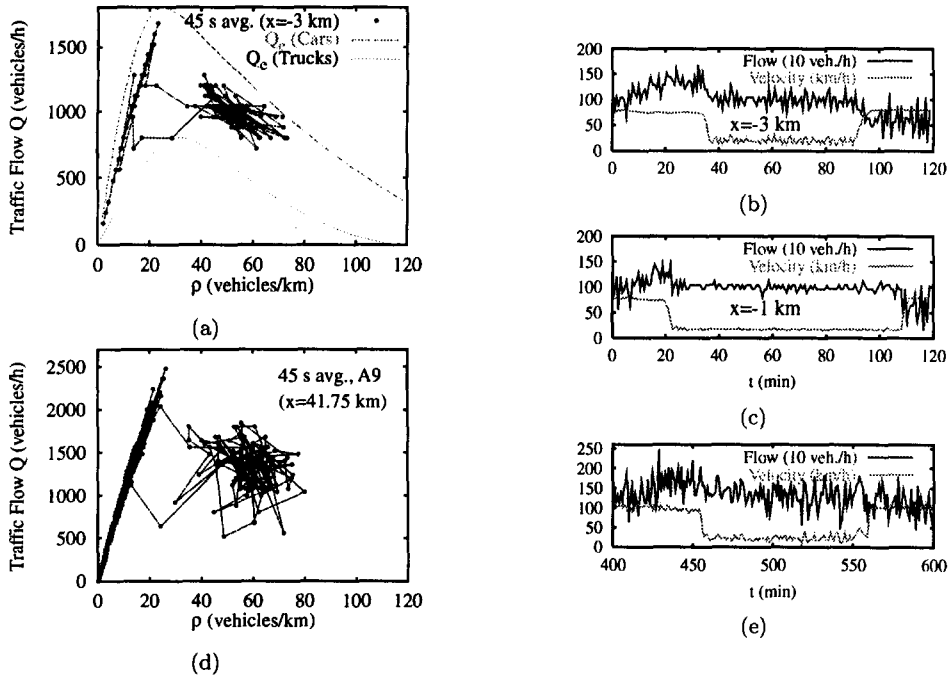

Figure 19. (a) Flow-density diagram and (b),(c) time series of single-lane heterogeneous traffic. (d),(e) Empirical data of extended congested traffic on the Dutch freeway A9.

sponds to a spatial coexistence of HCT and OCT. (For a pure OCT or TSG state, there would be no gap between the flow-density data of free and congested traffic, both in real traffic data and in simulations [67].)

4. MICRO-MACRO LINK

One of the biggest problems in comparing microscopic and macroscopic models via coarse graining is that a separation between the microscopic scale (of single vehicles) and the macroscopic scale (allowing us to determine densities and average velocities) is hardly possible. Either the averaging intervals are too small and aggregate quantities like the density cannot be defined consistently, or the averaging intervals are too large so that the dynamics of the model is smoothed out.

Generalizing an idea sketched in [51], we will now propose a way of obtaining macroscopic from microscopic traffic models, which is different from the gas-kinetic approach and (at least) applicable to the case of identical driver-vehicle units. For this, we define an average velocity by linear interpolation between the velocities of the single vehicles α,

$$V(x,t) = \frac{v_\alpha(t)[x_{\alpha-1}(t) - x] + v_{\alpha-1}(t)[x - x_\alpha(t)]}{x_{\alpha-1}(t) - x_\alpha(t)}, \tag{37}$$

where $x_{\alpha-1} \geq x \geq x_\alpha$, and the index α of driver-vehicle units increases against the driving direction. While the derivative with respect to x gives us

$$\frac{\partial V}{\partial x} = \frac{[v_{\alpha-1}(t) - v_\alpha(t)]}{[x_{\alpha-1}(t) - x_\alpha(t)]}, \tag{38}$$

the derivative with respect to t gives us the *exact* equation

$$\left(\frac{\partial}{\partial t} + V\frac{\partial}{\partial x}\right) V = A(x,t), \tag{39}$$

where

$$A(x,t) = \frac{a_\alpha(t)[x_{\alpha-1}(t) - x] + a_{\alpha-1}(t)[x - x_\alpha(t)]}{x_{\alpha-1}(t) - x_\alpha(t)} \tag{40}$$

is the linear interpolation of the single-vehicle accelerations a_α characterizing the microscopic model. For most car-following models, the acceleration function can be written in the form $a_\alpha = a_{\mathrm{mic}}(v_\alpha, \Delta v_\alpha, s_\alpha)$, where $\Delta v_\alpha = (v_\alpha - v_{\alpha-1})$ is the approaching rate, and $s_\alpha = (x_{\alpha-1} - x_\alpha - l_\alpha)$ the (netto) distance to the vehicle in front. In order to obtain a macroscopic system of partial differential equations for the average velocity and density, the arguments v_α, Δv_α, and s_α of the single-vehicle acceleration have to be expressed in terms of macroscopic fields as well. Specifically, we make the following approximations: $A(x,t) \approx a_{\mathrm{mic}}(V(x,t), \Delta V(x,t), S(x,t))$, with $\Delta V(x,t) = [V(x,t) - V_{\mathrm{a}}(x,t)]$, $S(x,t) = (1/2)[\rho^{-1}(x,t) + \rho_{\mathrm{a}}^{-1}(x,t)] - \rho_{\max}^{-1}$, and the nonlocality given by $g_{\mathrm{a}}(x,t) = g(x + 1/\rho(x,t), t)$ with $g \in \{\rho, V\}$. In this way, we obtain a nonlocal macroscopic velocity equation, which supplements the continuity equation (1) for the vehicle density and defines, for a given microscopic traffic model, a complementary macroscopic model. Note that it does not contain a pressure term $(1/\rho)\frac{\partial P}{\partial x}$ with $P = \rho\theta$, in contrast to the GKT model described above.

As Figure 20 shows for the intelligent driver model, there are microscopic models for which the above procedure leads to a remarkable agreement. First, we have simulated an open freeway stretch with the macroscopic counterpart of the IDM with given macroscopic initial and boundary conditions. Then, we have simulated the first three kilometers of the stretch microscopically with the IDM (Figure 20a, dark grey), using the same upstream boundary condition. As downstream boundary condition, we used the macroscopic simulation result at the interface ($x = 3\,\mathrm{km}$) to the remaining macroscopic simulation section (Figure 20a, light grey). The density profile at the interface is illustrated in Figure 20b. Figure 20c shows the density profile 1 km upstream of the interface obtained by the microscopic simulation, compared with that obtained from the separate macroscopic simulation of the whole system. The density $\rho(x,t)$ in the microscopic simulation section for $x_{\alpha-1} \geq x \geq x_\alpha$ was determined via the formula

$$\frac{1}{\rho(x,t)} = \frac{1}{\rho_{\max}} + \frac{s_\alpha(t)[x_{\alpha-1}(t) - x] + s_{\alpha-1}(t)[x - x_\alpha(t)]}{x_{\alpha-1}(t) - x_\alpha(t)}. \tag{41}$$

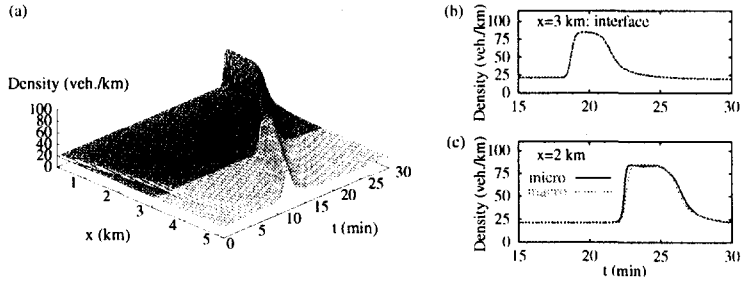

Figure 20. Results of simulations with the microscopic IDM (dark grey) and its macroscopic counterpart (light grey), assuming identical boundary and interface conditions.

The micro-macro link of traffic models is only of practical relevance if micro- and macrosimulations can be carried out *simultaneously*. For this, we have derived rules on how to translate macroscopic initial and boundary conditions into microscopic ones, with almost identical simulation results. In addition, we have developed methods to determine and apply the interface conditions (i.e., the respective upstream and downstream boundary conditions at interfaces) *dynamically* during the simulation, i.e., *on-line*. Since information must be able to flow through the interface in both directions, the formulation of dynamic interface conditions is a particularly tricky task which cannot be discussed here. Figures 21a and 21b show examples for the

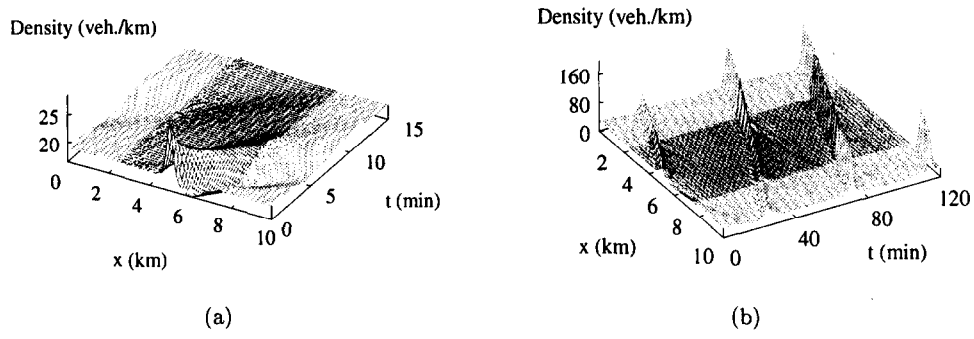

Figure 21. Results of simulations of a circular road, half of which was simulated microscopically (dark grey), while the other half was simulated macroscopically (light grey). Whereas the left picture shows the forward propagation of a decaying initial perturbation at small vehicle density, the right one illustrates the development of a backwards moving traffic jam at medium density.

spatiotemporal evolution of the density on a circular road. One half is simulated with the microscopic IDM (dark grey), and the other half is simulated with the macroscopic counterpart of the same model (light grey). As can be seen, it is possible to connect both sections in a way that small perturbations propagating in *forward* direction as well as developed density clusters propagating *backwards* can pass the interfaces without any significant changes in the shape or propagation velocity.

While traffic simulations with microscopic single-lane models are more intuitive and detailed than macroscopic simulations, a microscopic implementation of on- and off-ramps would require rather complex multilane models with lane-changing rules. Ramps can be treated much easier by macroscopic models, where they just enter by a simple source term in the continuity equation. Hence, the micro-macro link can be applied to combine both advantages. Figure 22 shows an open system that is simulated essentially with a microscopic single-lane model (dark grey). Only the ramp section (light grey) is simulated macroscopically. The on-ramp flow triggers a traffic breakdown to a triggered stop-and-go state, i.e., a cascade of traffic jams which propagate in the upstream microscopic section. The qualitative features of this complicated dynamics are in very good agreement with a purely macroscopic simulation of the same system.

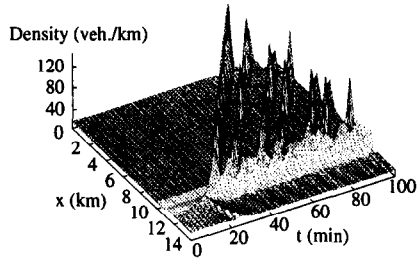

Figure 22. Result of a simultaneous micro-macro-simulation of triggered stop-and-go traffic, which is caused by high inflow from the ramp at $x = 11$ km. While the ramp section (light grey) is implemented macroscopically, the other two sections (dark grey) were simulated microscopically.

5. SUMMARY AND CONCLUSIONS

In this paper, we have shown that all presently known macroscopic phenomena of freeway traffic, including

(i) the fundamental diagram,
(ii) the characteristic parameters of congested traffic (outflow, propagation velocity, etc.), and
(iii) the transitions between free traffic, "synchronized" or other congested traffic, and stop-and-go traffic can be reproduced and explained by microscopic and macroscopic traffic models based on plausible assumptions and realistic parameters.

(iv) These models have also successfully reproduced a variety of empirical observations in a semiquantitative way, using the measured boundary conditions [55,67].

(v) Moreover, simply by simulating a mixture of different vehicle types, we obtained the observed scattering of congested flow-density data, although our traffic models are deterministic and have unique equilibrium relations.

(vi) Generalizations to multilane traffic [48,53] are expected to result in an even better agreement with empirical findings, e.g., a larger scattering of "virtual" detector data and flow-stabilizing effects of speed limits [77,78].

(vii) Finally, we established a link between microscopic and macroscopic models, which allows us to carry out simultaneous micro- and macro-simulations of neighboring freeway sections. To us, apart from developing measures for traffic optimization, the most interesting open question is which kind of observable phenomena are produced by the heterogeneity of driver-vehicle units *in addition* to the scattering of traffic data (see [6] for an example).

REFERENCES

1. W. Leutzbach, *Introduction to the Theory of Traffic Flow*, Springer, Berlin, (1988).
2. D. Helbing, *Verkehrsdynamik*, Springer, Berlin, (1997).
3. M. Schreckenberg and D.E. Wolf, Editors, *Traffic and Granular Flow '97*, Springer, Singapore, (1998).
4. P.H.L. Bovy, Editor, *Motorway Traffic Flow Analysis. New Methodologies and Recent Empirical Findings*, Delft University Press, Delft, (1998).
5. B.S. Kerner and H. Rehborn, Experimental properties of phase transitions in traffic flow, *Physical Review Letters* **49**, 4030–4033 (1997).
6. D. Helbing and B.A. Huberman, Coherent moving states in highway traffic, *Nature* **396**, 738–740 (1998).
7. B.S. Kerner and P. Konhäuser, Cluster effect in initially homogeneous traffic flow, *Physical Review E* **48**, R2335–R2338 (1993).
8. R.D. Kühne, Macroscopic freeway model for dense traffic—Stop-start waves and incident detection, In *Proceedings of the 9^{th} International Symposium on Transportation and Traffic Theory*, (Edited by I. Volmuller and R. Hamerslag), pp. 21–42, VNU Science Press, Utrecht, The Netherlands, (1984).
9. R.D. Kühne, Freeway speed distribution and acceleration noise—Calculations from a stochastic continuum theory and comparison with measurements, In *Proceedings of the 10^{th} International Symposium on Transportation and Traffic Theory*, (Edited by N.H. Gartner and N.H.M. Wilson), pp. 119–137, Elsevier, New York, (1987).
10. B.S. Kerner and P. Konhäuser, Structure and parameters of clusters in traffic flow, *Physical Review E* **50**, 54–83 (1994).
11. B.S. Kerner and H. Rehborn, Experimental properties of complexity in traffic flow, *Physical Review E* **53**, R4275–R4278 (1996).
12. D. Helbing and M. Treiber, Gas-kinetic-based traffic model explaining observed hysteretic phase transition, *Physical Review Letters* **81**, 3042–3045 (1998).
13. B.S. Kerner and H. Rehborn, Experimental features and characteristics of traffic jams, *Physical Review E* **53**, R1297–R1300 (1996).
14. B.S. Kerner, Experimental characteristics of traffic flow for evaluation of traffic modelling, In *Transportation Systems, Volume II*, (Edited by M. Papageorgiou and A. Pouliezos), pp. 793–798, International Federation of Automatic Control, Chania, Greece, (1997).
15. R.A. Raub and R.C. Pfefer, Vehicular flow past incidents involving lane blockage on urban roads: A preliminary exploration, In *77^{th} TRB Annual Meeting*, Manuscript No. 004, Transportation Research Board, Washington, DC, (1998).
16. H.Y. Lee, H.W. Lee and D. Kim, Phase digram of congested traffic flow: An empirical study, *Physical Review E* **62**, 4737–4741 (2000).
17. J. Treiterer and J.A. Myers, The hysteresis phenomenon in traffic flow, In *Proc. 6^{th} Int. Symp. on Transportation and Traffic Theory*, (Edited by D.J. Buckley), pp. 13–38, Elsevier, New York, (1974).
18. C.F. Daganzo, M.J. Cassidy and R.L. Bertini, Some traffic features at freeway bottlenecks, *Transportation Research B* **33**, 25–42 (1999).
19. B.S. Kerner, Experimental features of self-organization in traffic flow, *Physical Review Letters* **81**, 3797–3800 (1998).
20. M. Treiber, A. Hennecke and D. Helbing, Derivation, properties, and simulation of a gas-kinetic-based, non-local traffic model, *Physical Review E* **59**, 239–253 (1999).
21. M. Treiber and D. Helbing, Explanation of observed features of self-organization in traffic flow, Preprint, `http://xxx.lanl.gov/abs/cond-mat/9901239`.
22. D. Helbing, A. Hennecke and M. Treiber, Phase diagram of traffic states in the presence of inhomogeneities, *Physical Review Letters* **82**, 4360–4363 (1999).

23. M.J. Lighthill and G.B. Whitham, On kinematic waves: II. A theory of traffic on long crowded roads, *Proceedings of the Royal Society A* **229**, 317–345 (1955).
24. P.I. Richards, Shock waves on the highway, *Operations Research* **4**, 42–51 (1956).
25. G.F. Newell, A simplified theory of kinematic waves in highway traffic, *Transportation Research B* **27**, 281–313 (1993).
26. C.F. Daganzo, The cell transmission model: A dynamic representation of highway traffic consistent with the hydrodynamic theory, *Transportation Research B* **28**, 269–287 (1994).
27. D.F. Daganzo, The cell transmission model, Part II: Network traffic, *Transportation Research B* **29**, 79–93 (1995).
28. M. Hilliges and W. Weidlich, A phenomenological model for dynamic traffic flow in networks, *Transportation Research B* **29**, 407–431 (1995).
29. J.P. Lebacque, A finite acceleration scheme for first order macroscopic traffic flow models, In *Transportation Systems, Volume II*, (Edited by M. Papageorgiou and A. Pouliezos), pp. 815–820, International Federation of Automatic Control, Chania, Greece, (1997).
30. H.J. Payne, Models of freeway traffic and control, In *Mathematical Models of Public Systems, Volume 1*, (Edited by G.A. Bekey), pp. 51–61, Simulation Council, La Jolla, CA, (1971).
31. M. Papageorgiou, *Applications of Automatic Control Concepts to Traffic Flow Modeling and Control*, Springer, Berlin, (1983).
32. M. Cremer, *Der Verkehrsfluß auf Schnellstraßen*, Springer, Berlin, (1979).
33. W.F. Phillips, A kinetic model for traffic flow with continuum implications, *Transportation Planning and Technology* **5**, 131–138 (1979).
34. H.Y. Lee, H.W. Lee and D. Kim, Origin of synchronized traffic flow on highways and its dynamic phase transition, *Phys. Rev. Lett.* **81**, 1130–1133 (1998).
35. G.B. Whitham, *Linear and Nonlinear Waves*, Wiley, New York, (1974).
36. C.F. Daganzo, Requiem for second-order fluid approximations of traffic flow, *Transportation Research B* **29**, 277–286 (1995).
37. D. Helbing and M. Treiber, Numerical simulation of macroscopic traffic equations, *Computing in Science and Engineering* **1**, 89–99 (1999).
38. M. Bando, K. Hasebe, K. Nakanishi, A. Nakayama, A. Shibata and Y. Sugiyama, Phenomenological study of dynamical model of traffic flow, *Journal de Physique I France* **5**, 1389–1399 (1995).
39. D. Helbing and M. Schreckenberg, Cellular automata simulating experimental properties of traffic flow, *Physical Review E* **59**, R2505–R2508 (1999).
40. D. Helbing, Gas-kinetic derivation of Navier-Stokes-like traffic equations, *Physical Review E* **53**, 2366–2381 (1996).
41. D. Helbing, Derivation and empirical validation of a refined traffic flow model, *Physica A* **233**, 253–282 (1996).
42. I. Prigogine and R. Herman, *Kinetic Theory of Vehicular Traffic*, Elsevier, New York, (1971).
43. S.-L. Paveri-Fontana, On Boltzmann-like treatments for traffic flow. A critical review of the basic model and an alternative proposal for dilute traffic analysis, *Transportation Research* **9**, 225–235 (1975).
44. P. Nelson, A kinetic model of vehicular traffic and its associated bimodal equilibrium solutions, *Transport Theory and Statistical Physics* **24**, 383–409 (1995).
45. C. Wagner *et al.*, Second order continuum traffic flow model, *Physical Review E* **54**, 5073–5085 (1996).
46. A. Klar and R. Wegener, Enskog-like kinetic models for vehicular traffic, *Journal of Statistical Physics* **87**, 91–114 (1997).
47. P. Nelson and A. Sopasakis, The Prigogine-Herman kinetic model predicts widely scattered traffic flow data at high concentrations, *Transportation Research B* **32**, 589–604 (1998).
48. S. Hoogendoorn and P.H.L. Bovy, A macroscopic multi-lane multi-class traffic flow model, *79th TRB Annual Meeting 1999*, Washington (submitted).
49. A. Klar and R. Wegener, A hierarchy of models for multilane traffic I: Modeling, *SIAM Journal on Applied Mathematics* **59** (3), 983–1001 (1999).
50. A. Klar and R. Wegener, A hierarchy of models for multilane traffic II: Numerical investigations, *SIAM Journal on Applied Mathematics* **59** (3), 1002–1011 (1999).
51. D. Helbing, From microscopic to macroscopic traffic models, In *A Perspective Look at Nonlinear Media. From Physics to Biology and Social Sciences*, (Edited by J. Parisi *et al.*), pp. 122–139, Springer, Berlin, (1998).
52. D. Helbing and M. Treiber, Enskog equations for traffic flow evaluated up to Navier-Stokes order, *Granular Matter* **1**, 21–31 (1998).
53. V. Shvetsov and D. Helbing, Macroscopic dynamics of multi-lane traffic, *Physical Review E* **59**, 6328–6339 (1999).
54. D. Helbing, Empirical traffic data and their implications for traffic modeling, *Physical Review E* **55**, R25–R28 (1997).
55. M. Treiber and D. Helbing, Macroscopic simulation of widely scattered synchronized traffic states, *Journal of Physics A: Mathematical and General* **32**, L17–L23 (1999).
56. D. Helbing, Fundamentals of traffic flow, *Physical Review E* **55**, 3735–3738 (1997).
57. B.S. Kerner, P. Konhäuser and M. Schilke, "Dipole-layer" effect in dense traffic flow, *Physics Letters A* **215**, 45–56 (1996).

58. B.S. Kerner, P. Konhäuser and M. Schilke, Deterministic spontaneous appearance of traffic jams in slightly inhomogeneous traffic flow, *Physical Review E* **51**, R6243–R6246 (1995).
59. M.C. Cross and P.C. Hohenberg, Pattern formation outside of equilibrium, *Review of Modern Physics* **65**, 851–1112 (1993).
60. W.F. Ames, *Nonlinear Partial Differential Equations in Engineering, Volumes I & II*, Academic Press, New York, (1965).
61. W.H. Press, S.A. Teukolsky, W.T. Vetterling and B.P. Flannery, *Numerical Recipes in C: The Art of Scientific Computing*, Cambridge University Press, Cambridge, (1992).
62. C.F. Daganzo, M.J. Cassidy and R.L. Bertini, Possible explanations of phase transitions in highway traffic, *Transportation Research A* **33**, 365–379 (1999).
63. C.F. Daganzo, The nature of freeway gridlock and how to prevent it, In *Proc. 13th Int. Symp. on Transportation and Traffic Theory*, (Edited by J.B. Lesort), pp. 629–646, Pergamon-Elsevier, New York, (1996).
64. D. Helbing, Modeling multi-lane traffic flow with queuing effects, *Physica A* **242**, 175–194 (1997).
65. D. Helbing and M. Treiber, Jams, waves, and clusters, *Science* **282**, 2001–2003 (1998).
66. H.Y. Lee, H.W. Lee and D. Kim, Dynamic states of a continuum traffic equation with on-ramp, *Physical Review E* **59**, 5101–5111 (1999).
67. M. Treiber, A. Hennecke and D. Helbing, Congested traffic states in empirical observations and microscopic simulations, *Physical Review E* **62**, 1805–1824 (2000).
68. D. Helbing, A. Hennecke, V. Shvetsov and M. Treiber, Macroscopic traffic simulation based on a gas-kinetic, non-local traffic model, *Transportation Research B* **35**, 183–211 (2001).
69. A. Reuschel, Fahrzeugbewegungen in der Kolonne, *Österreichisches Ingenieur-Archiv* **4**, 193–215 (1950).
70. G.F. Newell, Nonlinear effects in the dynamics of car following, *Operations Research* **9**, 209–229 (1961).
71. M. Bando, K. Hasebe, A. Nakayama, A. Shibata and Y. Sugiyama, Dynamical model of traffic congestion and numerical simulation, *Physical Review E* **51**, 1035–1042 (1995).
72. P.G. Gipps, A behavioural car-following model for computer simulation, *Transportation Research B* **15**, 105–111 (1981).
73. S. Krauß, Microscopic modelling of traffic flow, Ph.D. Thesis, DLR, FB 98-08, Cologne.
74. D. Helbing and B. Tilch, Generalized force model of traffic dynamics, *Phys. Rev. E* **58**, 133–138 (1998).
75. R. Wiedemann, *Simulation des Straßenverkehrsflusses*, Institut für Verkehrswesen, Universität Karlsruhe, (1974).
76. See internet page `http://www.traffic-simulation.de`.
77. Interactive simulations of the multi-lane IDM are available at `http://www.uni-stuttgart.de/treiber/MicroApplet/`.
78. R. Sollacher and H. Lenz, Nonlinear control of stop-and-go traffic, In *Traffic and Granular Flow '99*, (Edited by D. Helbing *et al.*), Springer, Berlin, (2000).